# Sensitivity of the ANUBIS and ATLAS Detectors to Neutral Long-Lived Particles Produced in *pp* Collisions at the Large Hadron Collider

A THESIS PRESENTED
BY
THOMAS PEABODY SATTERTHWAITE
OF
PETERHOUSE
TO
THE DEPARTMENT OF PHYSICS

THIS THESIS IS SUBMITTED
FOR THE DEGREE OF
MASTER OF PHILOSOPHY

UNIVERSITY OF CAMBRIDGE
CAMBRIDGE, UNITED KINGDOM
AUGUST 2022

This thesis is the result of my own work and includes nothing which is the outcome of work done in collaboration except where specifically indicated in the text.

Thesis advisor: Professor Oleg Brandt Thomas Peabody Satterthwaite

# Sensitivity of the ANUBIS and ATLAS Detectors to Neutral Long-Lived Particles Produced in *pp* Collisions at the Large Hadron Collider

## Abstract

For the past fourteen years, the Large Hadron Collider (LHC) has been colliding particles at nearly the speed of light in an attempt to understand and test the Standard Model of particle physics. The Standard Model, however, is not a complete theory; for example, it lacks explanations for the observed matter-antimatter asymmetry, as well as for the nature of the dark matter which populates our universe. Many proposed extensions to the Standard Model postulate the existence of massive long-lived particles with lifetimes ranging up to one second. Despite their theoretical promise, however, searches for long-lived particles have yet to find experimental evidence.

This lack of observation may be due to a lack of sensitivity as the LHC's ATLAS Experiment alone is only sensitive to particles with proper lifetimes reaching about 10 ns. The ANUBIS project proposes installing a novel set of detectors in the existing service shaft of the LHC's ATLAS Experiment and/or in its cavern at a modest civil engineering cost. This thesis presents the ANUBIS project by discussing various proposed layouts for its detectors and the physics potential of these configurations. These studies show that the combined ANUBIS and ATLAS detectors could be sensitive to branching ratios of 10, 20, 30, and 40 GeV Higgs portal long-lived particle production reaching $\mathcal{O}(10^{-6})$ for particles with $c\tau$ of 3, 4, 6, and 10 m, respectively. This demonstrates an improvement of several orders of magnitude over the sensitivity of the ATLAS Experiment alone. Studies of the background events with which ANUBIS will have to contend are also presented, as is a discussion of its prototype detector, proANUBIS, which will seek to validate these studies.

# Contents

# Listing of figures

# Acknowledgments

THANK YOU to the many academics at the University of Cambridge and beyond who have been invaluable throughout this project, and my master's degree. Thank you especially to Prof. Oleg Brandt and Dr. Jonathan Burr for their guidance throughout this work, and for always pushing me to question my results and to dig deeper. Thank you also to Prof. Christopher Lester for his help along the way, and to the many individuals in Peterhouse who have shaped my postgraduate experience. Thank you to Dr. Giulio Aielli, Dr. Luca Pizzimento, Luigi Di Stante, Enrico Tusi, Dr. Sinem Sahin, and countless others for their selfless help in BB5 at CERN as we worked on constructing and commissioning the proANUBIS detector. Finally, thank you to the many professors and advisors at Harvard University, especially Prof. Melissa Franklin, who introduced me to the world of experimental high energy physics, and who gave me the tools to undertake this work and pursue the world of scientific research.

# 1

# Introduction

SINCE 2008, the Large Hadron Collider (LHC) has been colliding particles at close to the speed of light in an effort to measure the Standard Model and discover new physics. About one hundred meters below the surface of Geneva, Switzerland, the LHC accelerates particles, typically bunches of protons, around a ring measuring 27 km in circumference.[48] After reaching a speed of $.999999991c$, these bunches are collided every 25 ns, creating a deluge of new particles.[48] As these showers of particles are observed by one of the experiments around the LHC's ring, vast amounts of data telling of the physics at the high energy frontier of $\sqrt{s} = 13.6$ TeV are generated. Physicists working at the European Organization for Nuclear Research (CERN) then analyze this data and use it to scrutinize the Standard Model, hopefully finding hints of new physics: exotic phenomena which may tell of the nature of our universe.

Since its commissioning, physicists at CERN have used data from the LHC to make a number of landmark discoveries. In 2012, members of the ATLAS and CMS Experiments at CERN announced the detection of the Higgs boson, a fundamental particle that was theorized nearly fifty

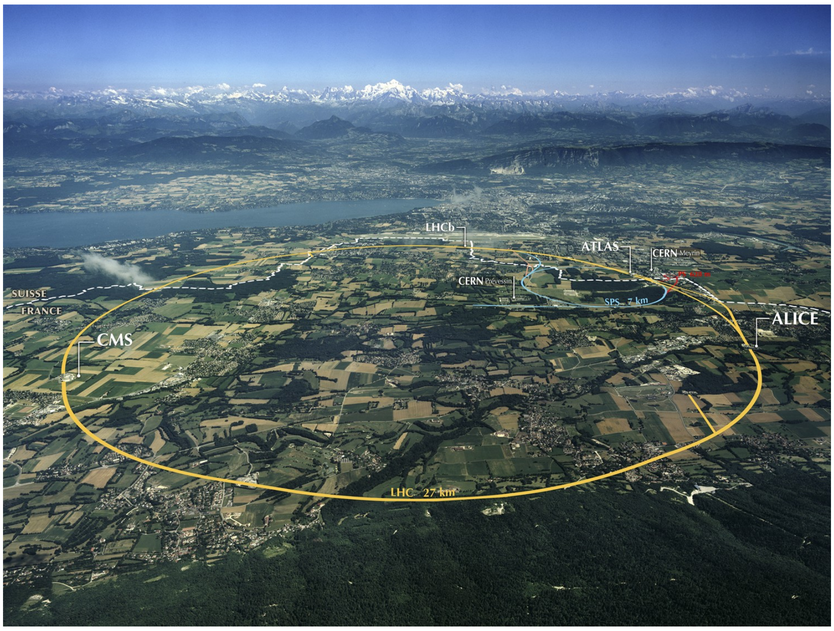


**Figure 1.1:** Aerial photograph of the Swiss-French border showing the ring of the LHC and the positions of its experiments. Source: CERN.[47]

years prior as an explanation for how matter obtains mass.[4] This discovery was quickly labeled one of the biggest scientific breakthroughs of the century, and it was the basis of the Nobel Prize in Physics awarded a year later.[83] Though it is the LHC's proudest accomplishment, the Higgs boson is far from the only particle discovered at the accelerator; as of writing, 67 new hadrons have been observed in collisions at the LHC.[74] This includes the most significant evidence yet for the existence of tetraquarks and pentaquarks, bound states of four and five quarks, respectively, with the latter having been first theorized nearly forty years prior to its observation.[79][6]

Despite this success, however, numerous questions still linger over the field of particle physics. The nature of dark matter, which comprises more than 80% of the universe's matter, is not known.[46] Albert Einstein's general theory of relativity has not been unified with the theory of quantum mechanics, yielding a conundrum known as the quantum gravity problem.[51] Neutrinos have been found to oscillate between lepton flavours, violating the Standard Model prediction that they are massless.[15] The observed asymmetry between matter and antimatter in our universe has no known origins.[63] It is not known why the weak force, which controls radioactive decay, is twenty-four orders of magnitude stronger than gravity, a discrepancy known as the hierarchy problem.[81]

Though they have been monumental in the field, the LHC's discoveries have not yet shed light on the answers to any of these open questions. Moving forward, the LHC's physics programme must therefore search for new phenomena in new ways in order to find new physics.

The Standard Model of particle physics describes the fundamental particles of the universe. It provides a mathematically elegant model for the known fermions and bosons and their interactions, however it does not include explanations for the aforementioned open questions.[69] A principle goal of the LHC's physics programme has been to test and constrain the Standard Model, and in this pursuit it has excelled; data collected by the collider has been found to be remarkably consistent with Standard Model predictions.[37] Some cracks have, however, emerged. A recent result from the LHCb Collaboration found a violation of lepton flavour universality in bottom quark decays significant to 3.1 standard deviations.[80] An earlier result from the LHCb Collaboration observed violation of charge conjugation parity symmetry in the decays of $B_s^0$ mesons with significance exceeding 5 standard deviations.[78] Extensions to the Standard Model are therefore necessary in order to explain these findings and answer open questions in the field without invalidating past results. Numerous potential extensions, known as Beyond the Standard Model (BSM) theories, have been proposed, however none have thus far gained significant experimental evidence.[76] Nevertheless, physicists continue to search for evidence of BSM phenomena as this would be a sign of new physics which could explain one or more fundamental questions.

Long-lived particles (LLPs) are a common feature of BSM theories. These are particles which, due to having a relatively small matrix element or phase space for decay, live for longer than most other particles before decaying.[76] This would allow LLPs travelling at close to the speed of light to travel deeper into detector material than most, and neutral LLPs could escape observation altogether by passing through existing detectors before interacting, therefore explaining why they have not yet been found. Supersymmetry (SUSY), for example, is a class of BSM theories which predicts novel LLPs. SUSY provides a mathematically compelling extension to the Standard Model by predicting a supersymmetric partner fermion for every known Standard Model boson, and vice versa.[81] This has been used to solve to the hierarchy problem, therefore leading to a large amount of interest in SUSY theories.[76] One theory, the Minimal Supersymmetric Standard Model (MSSM), gives rise to LLPs by describing the gravitino, a dark matter candidate, as the lightest supersymmetric partner

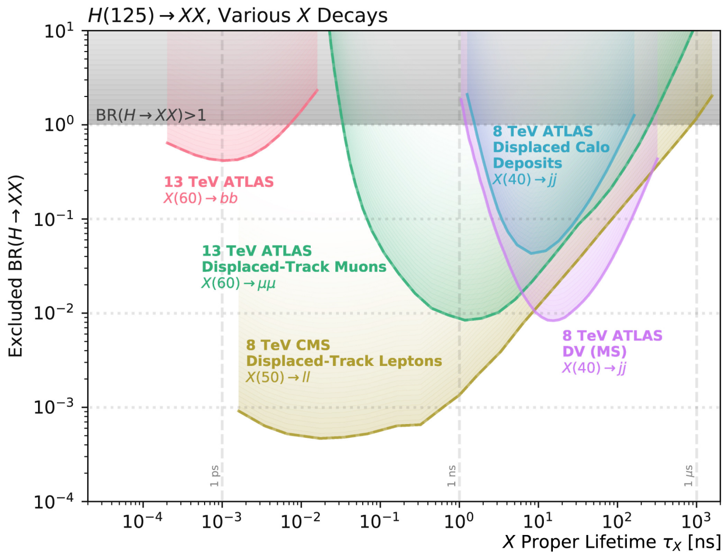


**Figure 1.2:** Excluded branching ratios of Higgs to LLP events at various proper lifetimes. Formed using recent LHC searches.[35 56 36 28 27] Source: Lee, L. et al.[76]

to a Standard Model particle, the theorized graviton.[59] It would therefore be the decay product of many MSSM particles, leading to ample production.

Many other theories which explain the nature of dark matter also predict the existence of LLPs. For example, the theory of freeze-in dark matter predicts a dark matter particle $\chi_1^0$ which is formed via the interaction $\chi_2^0 \rightarrow \chi_1^0 + X$ where $\chi_2^0$ is a particle in thermal equilibrium in the early universe, and $X$ is some number of Standard Model particles.[70] This interaction would be governed by a very weak coupling, therefore allowing $\chi_2^0$ to be long-lived.[76] Separately, asymmetric dark matter models postulate that the abundance of dark matter in our universe is related to the asymmetry between matter and antimatter.[92] This gives rise to operators which carry the asymmetry between the visible and dark sectors, and these operators are predicted by some supersymmetric theories. These operators would also govern the interactions of the corresponding lightest supersymmetric partner particle, which can again be long-lived.[76] Finally, exotic Higgs boson decays could yield LLPs via a so-called scalar portal model which would allow for the pair production of spin zero "hidden-sector" particles, which are also dark matter candidates.[96 97 52 54 53] These scalar particles could couple to Standard Model fermions and if prompt, hidden-sector decays are not permitted, they would be long-lived before decaying into these fermions.[58]

LLPs are clearly well motivated theoretically, and this has lead to numerous collider searches for their existence. These searches have probed a number of models of LLP production and have been sensitive to a range of LLP lifetimes, as shown in figure 1.2, however they have not yet found compelling evidence. For example, the ATLAS Collaboration searched for long-lived supersymmetric particles known as charginos by looking for a signature which appears only on the ATLAS Experiment's first set of detectors before the chargino decays into neutral or low-momentum particles which would escape detection. This search used $36.1\,\mathrm{fb}^{-1}$ of $pp$ collisions and was sensitive to particles with proper decay radii up to 300 mm, however it did not find a significant excess.[2] A separate analysis from the ATLAS Collaboration searched for Higgs portal-produced long-lived scalar particles which decay into bottom quarks, again with $36.1\,\mathrm{fb}^{-1}$ of data. This search used bottom quark jets to search for LLPs with $c\tau$ up to 6 mm, however it also did not find a significant excess.[35] The CMS Collaboration searched for similar Higgs portal LLPs using $137\,\mathrm{fb}^{-1}$ of data, this time also including decays of the scalar particle into $\tau$ leptons and down quarks. This search looked for jets in the CMS Experiment's end-cap muon detectors in order to be most sensitive to decays with proper decay lengths up to 40 m, however it did not find a significant excess.[98] Finally, a separate search from the CMS Collaboration used $19.6\,\mathrm{fb}^{-1}$ of data to look for LLPs which decay into pairs of electrons or muons, a process which has been predicted by some SUSY models. This analysis searched for displaced lepton vertices in order to be sensitive to LLPs with $c\tau$ ranging from 0.01 to 100 cm, however it again did not find a significant excess.[56] Other searches from the LHC's experiments have searched for a variety of BSM LLP models without finding compelling evidence.[40 5 39] LLPs have also been searched for using other accelerators, including the CDF and DZero Experiments at Fermi National Accelerator Laboratory and the BaBar Experiment at Stanford Linear Accelerator National Laboratory, all without finding significant experimental evidence.[42 77]

The lack of experimental evidence for LLPs may be due to a lack of experimental sensitivity. The ATLAS and CMS Experiments at the LHC were not designed with LLPs in mind, and they therefore do not include detectors more than about 10 m from their interaction points.[16 44] Neutral LLPs with lifetimes in excess of this distance could therefore traverse these experiments undetected and often decay into visible particles beyond the reach of existing detector acceptance. Given rare processes for the production of these particles, existing detectors could miss them altogether.

Modifications to these experiments are therefore necessary in order to maximize their sensitivity to exotic phenomena which may transcend the Standard Model. The forthcoming era of the High-Luminosity Large Hadron Collider (HL-LHC) will see the collider's luminosity increased roughly three-fold, allowing it to provide 3000 $\text{fb}^{-1}$ of data in the twelve years following the upgrade.[14] This upgrade could provide the most exciting potential for LLP production to date.[14] Equipped with new detector technology, LLP discovery potential could be radically increased without needing to build new accelerators like the Future Circular Collider or the International Linear Collider.[7, 66]

Currently, there are several proposals to extend the sensitivity of the LHC's experiments to LLPs. The MATHUSLA project proposes installing a large set of detectors on the surface above the LHC's CMS Experiment.[55] These detectors would begin roughly 60 m above the collider's beamline and be offset a further 70 m from the interaction point, making them sensitive to significantly displaced decays from neutral LLPs.[13] In order to cover a significant amount of solid angle at this distance, the detectors would fill a square building measuring 100 m on either side, beginning 20 m below the ground level and extending 9 m above it. This would be shielded from LHC-derived background events by the cavern material and earth between it and the interaction point, though the project would have to contend with cosmic muons and scattering atmospheric neutrinos. Its sensitivity to BSM phenomena is projected to peak at branching ratios probing $\mathcal{O}(10^{-5})$ for Higgs decays into 40 GeV LLPs with $c\tau$ of about $10^2$ m using HL-LHC conditions, a significant improvement over existing sensitivity.[55]

Separately, the CODEX-b project proposes installing a new set of detectors to a novel region of the LHCb Experiment's cavern.[67] This region previously held the experiment's data acquisition (DAQ) system, however this hardware has been moved to the surface level prior to the LHC's third run of data collection, leaving a 10 x 10 x 10 $\text{m}^3$ volume in which tracking detectors could be installed. These detectors would be located 26 m from the interaction point in the transverse coordinate, therefore making them sensitive to the displaced decays of neutral LLPs which otherwise would not have been observed by the LHCb Experiment's existing detectors. The project would have the key advantage of existing in a room which has already been shielded for the DAQ hardware, therefore limiting the number of background events which would penetrate this region. The room would also be able to hold more shielding material, should it be deemed necessary. This project would be maximally sensitive to exotic Higgs decays into LLPs with $c\tau$ of about 10 m, reaching sensitivity to branching ratios of dark photon production approaching $\mathcal{O}(10^{-4})$; again, this is a significant improvement over existing sensitivity.[67]

Finally, the ANUBIS project proposes installing a new set of detectors above the ATLAS Experiment, either along the ceiling of its cavern or in its PX14 service shaft.[43] These detectors would be located 23 to 80 m from the beamline, therefore allowing the project to search for decays which occur within the ATLAS Experiment's cavern and beyond its existing detectors, and potentially also within its PX14 service shaft. Its displacement from the LHC's beamline would make it particularly sensitive to the decays of LLPs in the mass range of 10 to 40 GeV, and its comparatively larger coverage in solid angle would give it impressive sensitivity.[43] Early-stage calculations project that detectors placed in the PX14 service shaft could have sensitivity to these particles with $c\tau$ of about 10 m reaching branching ratios of $\mathcal{O}(10^{-5})$, and it could be sensitive to particles with $c\tau$ of about $10^6$ m, which approaches the limit from Big Bang nucleosynthesis, before reaching the branching ratio limit of Higgs to invisible particle decays.[43] [64] This calculation, however, does not fully model LLP decay products and their interactions with ANUBIS, and it assumes that the project can operate as a background-free experiment, which may not be a valid assumption during HL-LHC conditions.

In order to further the ANUBIS project, these calculations must be refined. More detailed Monte Carlo simulations are necessary in order to better understand the project's sensitivity to BSM LLPs, both in its cavern ceiling configuration of detectors and in its PX14 service shaft configuration of detectors. Similar investigations of its sensitivity to the Standard Model LLPs which form the project's background are also necessary in order to fully understand the conditions in which ANUBIS would operate. These simulations allow for stronger statements to be made regarding ANUBIS' viability and physics potential, therefore making them vital for securing the scientific and financial support necessary to realize the project's new and exciting detectors. These simulations form the work that I have undertaken for my master's degree, which I present in this thesis.

This thesis is organized as follows. Section 2 presents an overview of the ATLAS Experiment and its existing detectors. Section 3 introduces the ANUBIS project and discusses the two proposed configurations for its detectors, which could be installed along the ceiling of the ATLAS Experiment's cavern or in its PX14 service shaft. Section 4 introduces the studies of Higgs portal BSM LLPs that I have carried out and presents results for ANUBIS' projected sensitivity to these phenomena, including comparisons to those of similar proposals. Section 5 presents similar studies of ANUBIS' sensitivity to the background events with which the project would have to contend during HL-LHC conditions.

A prototype detector, proANUBIS, has also been constructed at CERN to help calibrate estimates for the rate of background events within the ATLAS Experiment's cavern. This $180 \times 100\ \text{cm}^2$ array of resistive plate chamber detectors will be used to measure particle fluxes first on the surface above the ATLAS Experiment in 2022, then in its cavern beginning in 2023. Throughout my degree, I took a leading role in constructing and commissioning the proANUBIS detector, and this work is discussed in sections 3.3 and 3.4.

# 2

# The ATLAS Experiment

The ATLAS (A Toroidal LHC Apparatus) Experiment provides a general-purpose set of detectors which surround an interaction point of the LHC in a cavern roughly 100 m below the surface of Geneva, Switzerland. Using a range of tracking detectors and calorimeters, the experiment can provide measurements of the energies and trajectories of many of the particles which are produced by the LHC's high-energy *pp* collisions with nearly $4\pi$ steradian coverage.[16] Beginning with the layer closest to the interaction point, this is achieved using its inner detector comprised of a solenoid paired with a pixel detector, semiconductor tracker, and transition radiation tracker; its calorimeter comprised of an electromagnetic calorimeter and a hadronic calorimeter; and its muon spectrometer comprised of a toroidal magnet paired with thin gap chambers, cathode strip chambers, resistive plate chambers, and monitored drift tubes.[16] Each of these detector systems is split into a barrel region which curves around the beamline and two end-cap regions which form the bases at either end of the experiment's cylindrical shape to surround the interaction point with nearly complete coverage.[16]

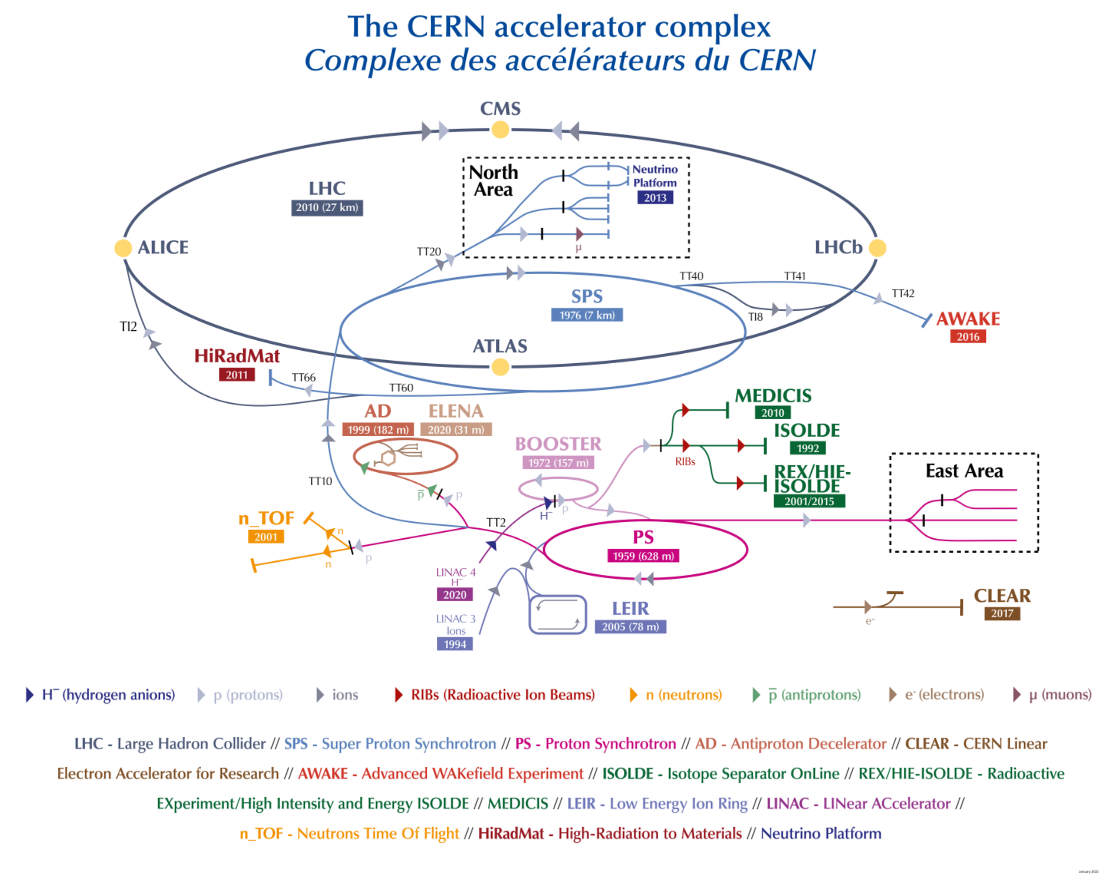


**Figure 2.1:** Drawing of the CERN accelerator complex showing the various rings used to accelerate beams of particles and feed them into the LHC's ring. Positions of the LHC's four interaction points are also shown. Source: CERN.[75]

## 2.1 Large Hadron Collider

The *pp* collisions observed by the ATLAS Experiment are generated by the LHC, a superconducting particle accelerator measuring 27 km in circumference which is located about 100 m underground.[48] The apparatus' two rings accelerate beams of particles in opposite directions to energies up to 7 TeV each, and collide them at several interaction points. The beams of particles, generally protons, are injected using a series of rings which form the accelerator complex. The complex begins with the Linear accelerator 4 (Linac4) which accelerates beams of negative hydrogen ions to energies reaching 160 MeV.[60] These beams then feed the Proton Synchrotron Booster (PSB) which strips the electrons from the hydrogen ions and accelerates them to 1.4 GeV before feeding them into the

Proton Synchrotron (PS). The PS then accelerates these protons to 25 GeV and feeds them into the Super Proton Synchrotron (SPS).[60] The SPS, a 7 km ring, finally accelerates the beams of protons to energies up to 449 GeV, at which point they are injected into the LHC.[60] This complex is shown in figure 2.1.

Once the beams of protons have been injected, the LHC uses a series of radiofrequency cavities and a 8.3 T magnetic field generated by supercooled dipole magnets to accelerate and guide the bunches of protons around its circular rings, reaching energies up to 7 TeV.[48] A 7.5 T field generated by supercooled quadrupole magnets is also used to focus the beams and increase their intensity.[93] These quadrupole magnets focus the beams in the vertical and horizontal directions, while sextupole and octupole magnets are also used to provide finer corrections which further intensify the beams. Once focused, the bunches, each of $1.2 \times 10^{11}$ particles, have a root mean square cross section of 16.7 $\mu$m and length of 7.6 cm.[48] This allows the LHC to reach a peak luminosity of $2 \times 10^{34}$ cm$^{-2}$s$^{-1}$, making it one of the highest luminosity particle accelerators in the world.[72]

After the beams of protons have reached their peak energies, they are crossed at a number of interaction points around the LHC where the accelerator's two rings share vacuum chambers. There are two high-luminosity interaction points, where the aforementioned peak luminosity is achieved, and these are surrounded by the ATLAS and CMS Experiments which are both general purpose detectors. At the ATLAS Experiment, which is the subject of this thesis, the beams are crossed in the vertical plane every 25 ns using a series of supercooled recombination and separation dipole magnets, which generate fields of 3.8 T and 1.4 T, respectively.[48] There are also two interaction points where slightly less focused beams are crossed, and these are surrounded by the LHCb and ALICE experiments. These are specialty experiments, with LHCb designed to probe the physics of bottom quarks, and ALICE designed to study heavy ion collisions when the LHC accelerates lead nuclei rather than protons.[48]

## 2.2 Inner Detector

Following a *pp* collision, the ATLAS Experiment's inner detector system provides tracking and momentum measurements of the prompt particles. Its first set of detectors, the pixel detectors, provide the most precise tracking measurements. Four layers of pixel modules are arranged along the bar-

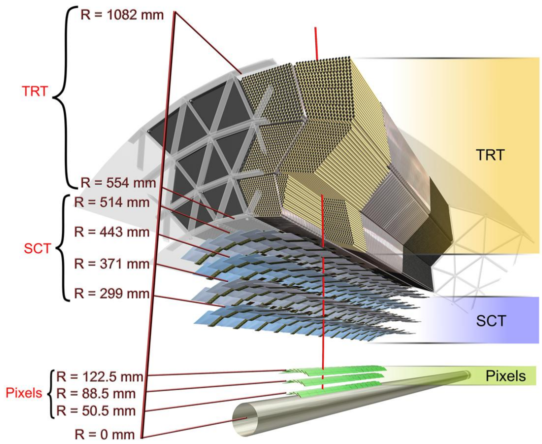


**Figure 2.2:** Schematic of how the pixel detector, semiconductor tracker, and transition radiation tracker form the inner detector and observe an incoming particle. Note that a fourth layer of pixel detectors was installed at $R = 33.25$ mm following the LHC's first run of data collection.[91] Source: CERN.[87]

rel region at distances of 33.25 mm to 122.5 mm from the beamline, and three layers of modules are placed in both end-cap regions, each at distances of 495 mm to 962 mm from the interaction point.[91 100] The three outer layers in the barrel and end-cap regions use silicon pixels measuring 50 x 400 $\mu$m$^2$ and the innermost barrel layer uses silicon pixels measuring 50 x 250 $\mu$m$^2$ to produce measurements with a precision of roughly 8 $\mu$m.[91] In addition to providing the ATLAS Experiment's most precise tracking capabilities, these silicon detectors can also provide measurements of the energy deposited by a particle as it traverses the detector. This yields a measurement of the change in this quantity as the particle travels across the pixel layers, known as its $dE/dx$.[23] Measurements of $dE/dx$ have been used for particle identification as the Bethe-Bloch formula relates this quantity to the particle's momentum.[102 41]

Following the pixel detector is the inner detector's coarser semiconductor tracker. Strips of silicon are arranged at distances of 300 mm to 520 mm along the barrel region, with nine end-cap modules ranging from 853.8 mm to 2720.2 mm away from the interaction point on either side.[26] As a charged particle passes across the semiconductor tracker's doped silicon strips, it generates an electric charge which can be read out as signal. Readout strips are installed every 80 $\mu$m along the silicon, allowing for measurements of particle tracks with a precision of roughly 23 μm.[71] This aids in the measurements from the pixel detectors, and it can be used to reconstruct vertices from decays of particles which have already traversed earlier layers.

The final component of the inner detector is its transition radiation tracker which uses gaseous detectors to measure particle trajectory and identify particle flavour. Thin tubes of readout wires paired with xenon- and argon-based gaseous mixtures are arranged from a distance of 560 mm to 1080 mm from the beamline along the inner detector's barrel region extending up to 720 mm from the beamline, and along a distance of 827 mm to 2774 mm from the interaction point in each of the end-cap regions extending from 617 mm to 1106 mm from the beamline.[82] In addition to providing tracking measurements with a precision of 0.1 mm, these detectors can help identify particles by measuring their transition radiation as they traverse the detector.[25, 82] Together, these three technologies allow the inner detector to observe prompt, potentially short-lived particles produced in a *pp* collision, and to identify vertices.[19] The system is immersed in a 2.6 T field produced by the central solenoid magnet which deflects the trajectories of charged particles as they travel.[20] By using its tracking detectors to measure the radius of curvature as a particle is deflected, the inner detector can also produce a measurement of momentum.[16] A schematic of how this system observes particles is shown in figure 2.2.

## 2.3 Calorimeters

Following the ATLAS Experiment's inner detector, its calorimeters provide measurements of the energies of traversing particles. The electromagnetic calorimeter consists of layers of tungsten, copper, and lead which absorb incoming electrons, photons, and jets.[101] These absorptions generate showers of secondary particles which create a measurable electric current after ionizing liquid argon, and this occurs in a region with a thickness of 53 cm along 6.8 m of the barrel.[101, 17] Beyond the electromagnetic calorimeter lies the hadronic calorimeter which provides measurements of the energies of particles which do not deposit all of their energy in the electromagnetic calorimeter. Using plastic scintillators, it measures the secondary particles produced by collisions with layers of steel, and it extends 5.64 m along the beamline with a thickness of 195 cm.[18] Both of these technologies also appear in the end-cap region, with the liquid argon calorimeter again closer to the beamline.[16] To-

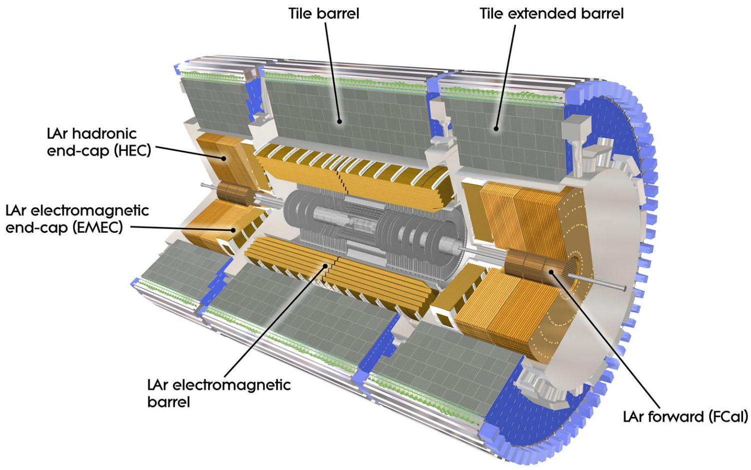


**Figure 2.3:** Schematic showing the components of the calorimeter. Source: CERN.[86]

gether, these technologies measure 9.7 radiation lengths at $\eta = 0$, which significantly attenuates the number of jets which appear in further parts of the experiment.[57] They have also been shown to measure the energies of reconstructed jets with a resolution of $52\%/\sqrt{E}$.[57] This system is shown in figure 2.3.

## 2.4 Muon Spectrometer

Finally, the experiment's muon spectrometer provides measurements of the trajectories and momenta of muons, which are unlikely to interact with the experiment's inner detector or calorimeters.[69] Thin gap chambers and resistive plate chambers provide triggering capabilities as well as measurements of trajectories in $\varphi$, the azimuthal angle around the beamline.[21] Both of these technologies use layers of charged plates surrounding gaseous mixtures. As a muon traverses these gases, it ionizes the gas and produces electrons which are drawn to the charged plates, therefore creating a measurable electric current.[84] Similarly, cathode strip chambers use charged wires placed in a gaseous mixture to measure the $\eta$ coordinate, which is analogous to the polar angle with the beamline, of muon trajectories with a precision of 60 $\mu$m.[62] Monitored drift tubes again use a gaseous mixture which is ionized by traversing muons, and the ensuing electric charge is read out by wires which pass through tubes of the gas.[21] This technology is necessary for precisely measuring the $\eta$

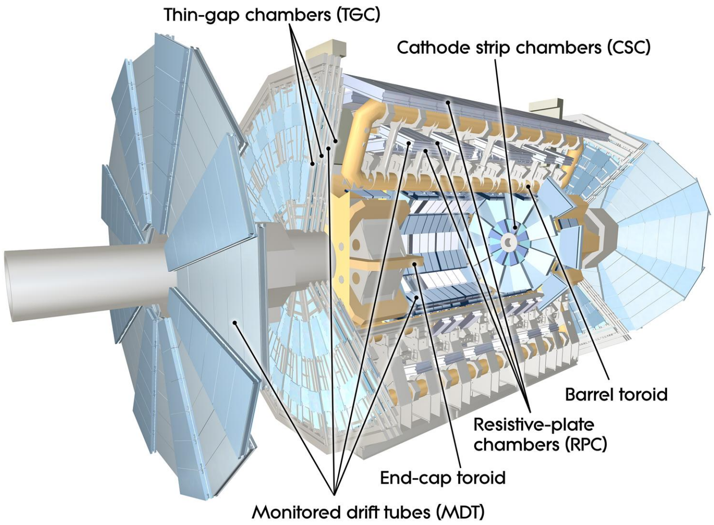


**Figure 2.4:** Schematic showing how the end-cap and barrel toroids and the cathode strip chambers, monitored drift tubes, thin-gap chambers, and resistive-plate chambers form the muon spectrometer. Source: CERN.[88]

coordinate of a particle's trajectory, which it does with a resolution of 60-70 $\mu$m.[62]

Together, these technologies, along with the experiment's magnetic field, form the muon spectrometer, which is shown in figure 2.4. The experiment's toroidal magnet, which extends from 4.7 m to 10.1 m from the beamline in the barrel region, uses eight coils to generate a magnetic field peaking at 3.9 T.[20] As muons pass through this field, their nonzero electric charge causes their trajectories to deflect in $\eta$. Measuring this curvature, by using tracking detectors to measure the sagitta of the particle's path, therefore provides a momentum measurement.[69] This explains why $\eta$ is referred to as the "precision" coordinate in the muon spectrometer; while there should be a symmetry in $\varphi$, the $\eta$ measurement tells of the energy of a particle, and therefore its precision is paramount. This is the same principle which is used in the inner detector, where the central solenoid magnet generates a field up to a 2.6 T to aid in measuring the momenta of prompt particles.[20]

## 2.5 Trigger and Data Acquisition

While the various detectors and calorimeters of the ATLAS Experiment are capable of measuring the energies and trajectories of the particles which are produced in a *pp* collision, it is still necessary to determine whether this data should be saved in a given event. Bunches of protons are crossed

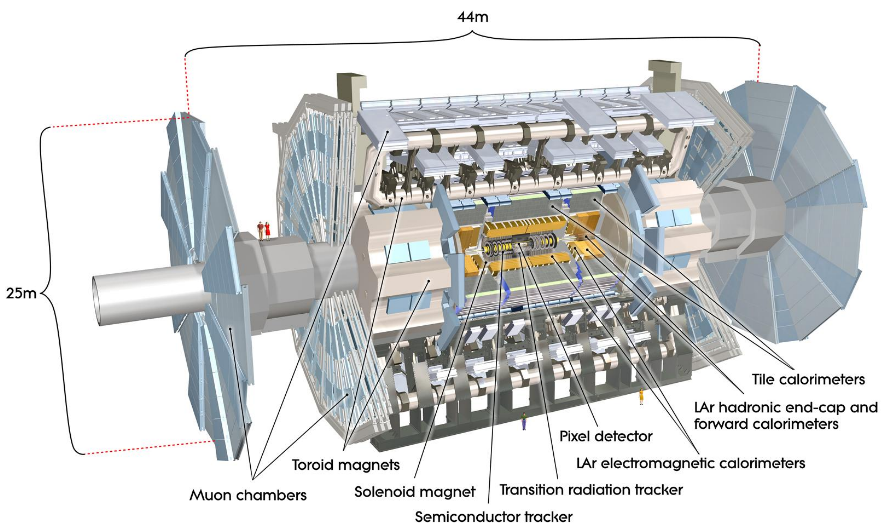


**Figure 2.5:** Schematic of the full ATLAS detector with its various detectors and subsystems labelled. Source: CERN.[89]

every 25 ns, so there are clear technical and storage limitations to reading out and saving every collision.[30] The experiment's trigger system determines which events are of interest, and its data acquisition system saves these events. This system seeks to reduce the rate of events which are output from the bunch crossing frequency of 40 MHz to a frequency of about 1 kHz.[38] The system begins with a hardware-based level 1 trigger, which uses the Central Trigger Processor, a system supplied with signals from the calorimeter and muon subsystems, to quickly determine if an event may be of interest.[49] The output of this trigger is then supplied to the high level trigger, which uses a software-based level 2 trigger and Event Filter to further reduce output rates.[49] These systems use a range of criteria to determine if an event's contents should be recorded including, for example, the presence of certain flavours of particles or certain signatures in the detectors.[49] Finally, the data logger records events passing the trigger criteria so that they may be analyzed at a later date.[99]

## 2.6 Preparations for the High-Luminosity Large Hadron Collider

In preparation for the era of the HL-LHC, the ATLAS Experiment's detectors and trigger system are being significantly upgraded. During Run 4 of data collection, the LHC aims to reach a peak luminosity of $5 \times 10^{34}$ cm$^{-2}$s$^{-1}$, a roughly three-fold increase from its Run 2 luminosity.[14] With this increased luminosity comes increased experimental challenges; interactions between beam particles and beam pipe material, known as beam halo, and radiation from jet-produced scattering neutrons are both expected to increase in frequency, and therefore degrade existing detectors at an increased rate.[94 68] To cope with these challenges, the ATLAS Experiment's detectors are being upgraded in two phases, one during Long Shutdown 2 prior to Run 3 of data collection, and one during Long Shutdown 3 prior to Run 4, the first of the HL-LHC.[14]

Phase I of upgrades saw the installation of the New Small Wheels, which are new end-cap detectors, and the first cells of the BIS78 resistive plate chambers, which are new barrel detectors, to the muon spectrometer, as well as upgrades to the liquid argon calorimeter.[73 32 9] The trigger and data acquisition system was also upgraded to maintain previous trigger rates despite the higher luminosity.[33] During phase II of upgrades, more muon detectors will be replaced in the barrel and inner end-cap regions using the BIS78 technology, and a new silicon inner tracker, called the ITk, will be installed to replace the pixel and semiconductor trackers.[32 31] Readout electronics for the electromagnetic calorimeter will also be upgraded, as will parts of the hadronic calorimeter, and the trigger and data acquisition system.[29 34 33]

The ATLAS Experiment's detectors, which have near full coverage in solid angle, and triggers, which use a broad range of criteria to output events, make it a general-purpose detector as it lacks bias towards observing only a specific type of particle or interaction.[16] As shown in figure 2.5, it completely surrounds an interaction point of the LHC, and it is well equipped to measure the energies and trajectories of the Standard Model particles produced therein. It is also believed to be well equipped to measure particles predicted by BSM theories, however evidence for these particles has not yet been observed.[76] This may be because it lacks sensitivity to neutral BSM particles which travel a significant distance before decaying.[43] In the barrel region, the experiment's detectors extend to a distance of 12.5 m from the beamline, with vertex reconstruction efficiency dropping dramatically after a limit of about 7.5 m due to sparse detector coverage beyond this point, so any decay after this limit would likely go undetected.[21 3] Extensions to the experiment are therefore desirable in order for it to reach its full potential in observing the decays of BSM LLPs. Phase II of upgrades prior to the HL-LHC provides an excellent opportunity to undertake the installation of a novel set of detectors which would address this lapse in sensitivity to potentially exotic phenomena.

# 3

# The Proposed ANUBIS Experiment

The ANUBIS (An Underground Belayed In-Shaft Search Experiment) project proposes installing a new set of detectors to a novel location in the ATLAS Experiment's underground cavern in order to increase the experiment's sensitivity to the decays of neutral LLPs.[43] The vertexing limit of the ATLAS Experiment's muon spectrometer lies at roughly 7.5 m from the beamline, so any decays which occur beyond this point would not be observed.[3] If the progenitor of these decays were to be a neutral particle, then it would traverse the ATLAS Experiment without interacting with its inner detector, calorimeter, or muon spectrometer.[43] Therefore, the installation of new detectors further from the interaction point would extend the experiment's sensitivity to this phenomena, which could be indicative of physics which transcends the Standard Model.[43] By capitalizing upon the existing civil engineering of the ATLAS Experiment's cavern, the ANUBIS project seeks to provide this sensitivity at a modest cost; initial estimates for installing tracking detectors to the ATLAS Experiment's PX14 service shaft calculate a project cost of about €10 M.[43]

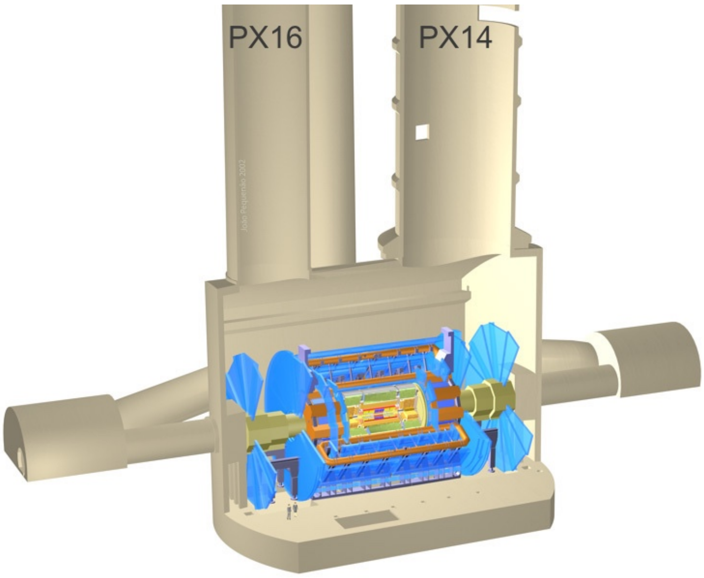


**Figure 3.1:** Drawing of the ATLAS Experiment in its cavern with the positions of the PX14 and PX16 service shafts labelled. Source: CERN.[90]

## 3.1 Potential Layouts

The ANUBIS project proposes two potential configurations for its detectors. A "ceiling" configuration proposes installing detectors which cover the curved ceiling of the ATLAS Experiment's cavern, extending 53 m along the beamline and 15 m in both horizontal directions. This would include detectors which cover the PX14 and PX16 service shafts, which are shown in figure 3.1, and it would provide the greatest coverage in solid angle while searching for decays which occur between the ATLAS Experiment's vertexing limit and the new detectors.[61] A "shaft" configuration proposes installing a set of detectors at various locations in the PX14 service shaft. These would be arranged as four circular tracking stations, each of which would be belayed to a different height along the extent of the shaft.[43] Tracking stations with radii of 8.75 m would be installed at 23, 42.5, 61.3, and 80 m above the LHC's beamline, beginning 4.5 m along the beamline from the interaction point. This would limit the project's coverage in solid angle, however it would provide coverage which extends significantly further from the interaction point as it searches for decays between the ATLAS Experiment's vertexing limit and its first tracking station, or between its tracking stations. These two configurations are shown in figure 3.2.

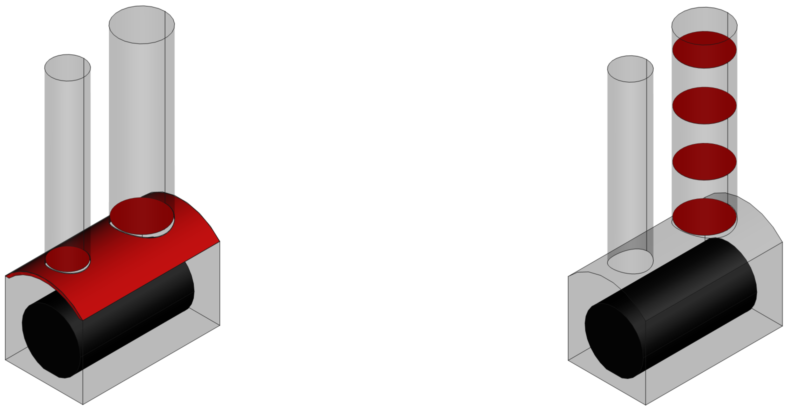

**(a)** Ceiling geometry

**(b)** In-shaft geometry

**Figure 3.2:** Schematics showing both proposed layouts for the ANUBIS project. The ATLAS Experiment is shown as a black cylinder with ANUBIS' RPC detectors shown in red, either (a) along the ceiling of the cavern or (b) in the PX14 service shaft. Source: Olivia Valentino.

## 3.2 Tracking Stations

Each potential layout for ANUBIS seeks to capitalize upon the recently-developed BIS78 resistive plate chamber (RPC) technology. These detectors have been commissioned in order to upgrade the barrel region of the ATLAS Experiment's muon spectrometer, and they are being piloted during Run 3 of data collection in preparation for the forthcoming era of the HL-LHC.[14] The new detectors use copper strips with a 25 mm pitch in order to achieve hit resolution of 1 mm, and they use a higher electric potential (6000 V) across a thinner (1 mm) gas gap than previous RPC generations in order to provide timing resolution of roughly 0.5 ns.[32] As the ATLAS Experiment looks to produce and commission a large number of these detectors during Phase II of its upgrades, the ANUBIS project hopes to capitalize on this effort to produce its tracking stations.[43]

Each ANUBIS tracking station would have six layers of these BIS78 RPCs. These would be arranged into two triplets spaced roughly 1 m apart, where a triplet consists of three RPC singlets spaced about 1 cm apart.[43] A singlet contains two RPC panels, one with readout stripes running perpendicular to the other, which are mounted to opposite sides of a gas gap measuring 1 mm.[32] This allows each singlet to measure a hit's position in two dimensions beyond the panels' fixed positions, and it allows each triplet to measure a particle's trajectory as hits from different singlets are stitched together during data analysis. Using three RPC singlets in each triplet allows for sufficient

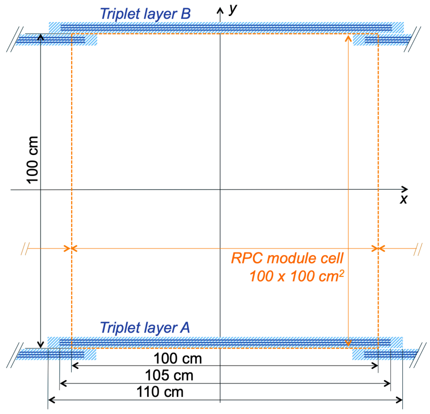


**Figure 3.3:** Cross section of an ANUBIS tracking station cell showing the relative positions of BIS78 RPC singlets and triplets. Each triplet contains three singlets, each of which consists of a gas gap and strip panels which produce measurements in perpendicular directions. Overlap between the fiducial areas of triplets on adjacent tracking station cells is shown. Source: Bauer, M. et al.[43]

discrimination against noise as three colinear hits in each dimension are unlikely to come from random noise, and it also provides sufficient redundancy should a given panel fail to register the passage of a charged particle.[32] Placing each triplet 1 m apart also gives a sufficient lever arm so that a particle's slope can be resolved as it passes across the tracking station.[43]

The BIS78 RPCs for ANUBIS tracking stations would likely be produced in 1 $m^2$ cells, as shown in figure 3.3, which would then be arranged into the irregular shapes of the tracking stations: circles for the in-shaft configuration or curved sheets for the ceiling configuration. This could be achieved by overlapping adjacent RPC cells so that there is at least a 5 cm overlap in the fiducial region along any given side of the detector.[43] In the case of the ceiling configuration, this would also involve adding a slight incline in order to match the curvature of the ceiling of the ATLAS Experiment's cavern. In the case of the in-shaft configuration, it may also be necessary for tracking stations to have foldable or retractable cells so that their footprints could be minimized while they are stored at the surface level prior to deployment to the PX14 service shaft, or during a routine removal. Work investigating the feasibility of this type of novel detector structure is ongoing.

In the scenario of the cavern ceiling configuration, the RPC tracking stations could be installed directly to the ceiling of the ATLAS Experiment's cavern. At the bottoms of the PX14 and PX16 service shafts, however, circular tracking stations would have to be installed where there is no ceiling, and these would be belayed from the surface level to a height of 23 m above the LHC's beamline. Similarly, the in-shaft scenario involves four tracking stations which would each be belayed from the surface level to heights of 23, 42.5, 61.3, and 80 m above the LHC's beamline. These tracking stations would include a small cutoff to allow for unobstructed passage of the ATLAS Experiment's pipework, as shown in figure 4.3.[43] Belaying the tracking stations would provide a cost-effective solution for installing the detectors with sufficient stability so that they remain stationary during a run of data collection at the LHC, while also providing the ability to quickly remove the devices and provide unrestricted access to the ATLAS Experiment in the event of an emergency.[43] Upon removal, the tracking stations could be stored at the surface level, perhaps in the aforementioned folded or retracted state in order to minimize their footprint, so that the existing detectors of the ATLAS Experiment could be serviced as usual. Work to understand the cost of developing this type of novel detector structure, as well as the time and risk involved with installing and removing the tracking stations, is ongoing. This is important for ensuring that ANUBIS is complementary to the ATLAS Experiment without detracting from its existing physics programme.

A key advantage of either of these potential ANUBIS configurations is that their proximity to the ATLAS Experiment would allow them to be integrated with its level 1 trigger. At HL-LHC conditions, the level 1 trigger seeks to realize a latency of 10 $\mu$s.[33] Given that the furthest tracking station is located roughly 70 m above the ATLAS Experiment's barrel, this latency could be achieved by the relatively short length of cable needed to connect the detectors' triggers.[43] This means that a signal in ANUBIS could trigger the readout of an event observed by the ATLAS Experiment, therefore aiding the search for decays of neutral LLPs. It would also allow ANUBIS to trigger on certain signatures in an event which are likely to be correlated with BSM LLP production, such as a high amount of missing energy in the transverse direction.[43] Furthermore, it could also potentially allow for new triggers which would enhance searches in the scope of the ATLAS Experiment's existing physics programme.

## 3.3 proANUBIS Construction and Commissioning

Prior to commissioning the full set of detectors for the ANUBIS project, it is imperative to understand the background events which exist in the ATLAS Experiment's cavern. Section 5 discusses

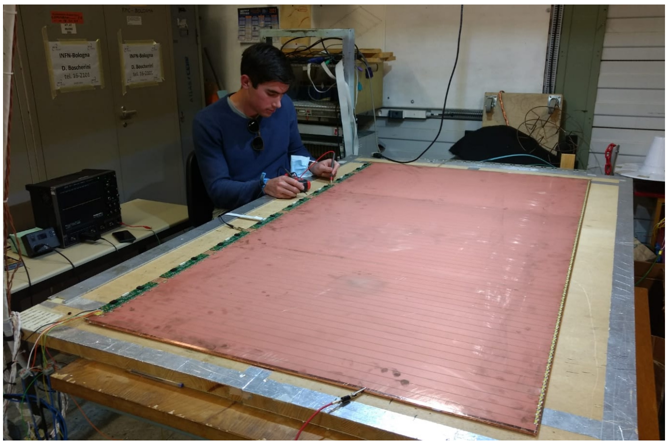

**Figure 3.4:** Testing the conductivity of a soldered connection between a BIS78 front-end board and a strip panel for use in a proANUBIS singlet.

initial calculations for the number of neutron and long-lived neutral kaon interactions that may be present in this region, however it is still necessary to verify these estimates and to determine if there are other types of events which have not yet been identified as sources of background. To aid in this pursuit, a prototype ANUBIS detector, named proANUBIS, is being constructed and commissioned at CERN. This prototype emulates one cell of an ANUBIS tracking station by consisting of six BIS78 RPC singlets measuring $180 \times 100$ cm$^2$. Beginning in late 2022, the detector will be placed on the surface level above the concrete beams which close-out the PX14 service shaft during runs of data collection, with the goal of moving proANUBIS to the ATLAS Experiment's cavern in 2023 so that it may collect data closer to the interaction point. This will allow the detector to measure particle fluxes from punch-through jets and secondary interactions within the ATLAS Experiment's cavern, and it will provide data which helps understand the amount of shielding provided by the concrete beams which close-out the PX14 shaft.

Work on proANUBIS began in February 2022 with the construction of its BIS78 RPC singlets, and it continued over the course of several trips that I took to CERN during my master's degree. To begin, prefabricated 25 mm pitch strip panels were prepared. Each panel measures $180 \times 100$ cm$^2$ and two such panels, with strips running in perpendicular directions, compose one singlet. Each singlet has one panel with 64 strips running along the short (100 cm long) dimension, with the other having 32 strips running along the long (180 cm long) dimension, along with some non-fiducial

**Figure 3.5:** Stack of BIS78 RPC strip panels for proANUBIS' singlets, after having their termination resistors and front-end boards installed.

area on each panel for the readout electronics. These panels were prepared by soldering termination resistors to one end of each strip, in order to match impedance and eliminate signal reflection, and front-end boards to the other end of each strip, in order to read out signal. This used proprietary front-end boards which were designed and built for use with CERN's BIS78 RPC detectors, each of which collects the electric signals from eight strips. After preparation, these panels were tested by evaluating their front-end boards' abilities to read a simple inductive signal, which was produced by touching a finger to each strip one-at-a-time, to ensure that there were no major defects in the panels or their electronics. This test showed promising results, finding that more than 99.5% of the singlets' strips read out a signal when their front-end boards were connected to an oscilloscope. This work was carried out in collaboration with Dr. Jonathan Burr and Prof. Oleg Brandt, and it was advised by many members of the ATLAS Experiment's BIS78 RPC team.

Pairs of RPC panels with strips running in perpendicular directions were then assembled into singlets by installing their gas gaps. The prefabricated 1 mm gas gaps and high voltage panels were installed between pairs of strip panels, with each panel having its strips facing the gas gap. This was achieved by placing an insulating material between the gas gap's bakelite and the strip panels, then wrapping the singlet's perimeter with a layer of aluminum tape. The insulating material shields the panels' strips from the gas gap's high voltage, and the aluminum tape creates a Faraday cage around the singlet in order to protect adjacent singlets from noise.[32] Sufficient grounding of singlets' electronics is also necessary in order to minimize noise across the detector, so the ground terminal for each strip on each front-end board was also soldered to the ground of its facing panel on the singlet. This work was again carried out in collaboration with Dr. Jonathan Burr and Prof. Oleg Brandt, and it was advised by the ATLAS Experiment's BIS78 RPC team.

With proANUBIS' singlets constructed, it was then necessary to test their abilities to register the hits of traversing particles in order to commission the detector. This was carried-out by measuring a triplet's track reconstruction efficiency with cosmic muons. Cosmic muons with $E > 1$ GeV should pass through a proANUBIS singlet's fiducial region with a frequency on the order of $10^2$ Hz, so they therefore provide an excellent source of signal with which to test the detector. [102] A separate trigger, such as a scintillator, was not available for data collection, so signal from proANUBIS' front-end electronics was read out whenever there was a signal detected by one of its boards. A muon was then considered reconstructed during this event of data collection when colinear hits were measured by each of a triplet's six strip panels, signifying a measurement of the particle's trajectory. The efficiency of a given panel was calculated to be how often, i.e. in what fraction of events, that panel registered a hit which was aligned with the triplet's other panels' registered hits. This measurement was carried out for the panels of one of proANUBIS' triplets, and this was done in collaboration with Dr. Jonathan Burr and Prof. Oleg Brandt using data analysis scripts provided by the ATLAS Experiment's BIS78 RPC team.

In order to best understand the performance of proANUBIS' singlets, its layers' efficiencies were measured with a range of high voltages supplied to their gas gaps. That is, one singlet's high voltage was toggled while the triplet's other singlets were kept at the standard high voltage of 6000 V, and the efficiency of the toggled singlet was considered. This began at the standard high voltage of 6000 V and probed voltages down to 5200 V, at which point efficiency was observed to drop-off considerably. 10 minutes of data were collected for the 6000 V benchmark, and 3 minutes of data were collected for each of the lower-voltage benchmarks as the statistics were found to stabilize at that point. Results of this analysis for one of proANUBIS' triplets can be seen in figure 3.6. Efficiency is observed to drop-off significantly when high voltage is lowered to 5200 V, with the highest value registering 0.67 for the middle singlet's 64-strip panel. At 6000 V, it peaks at values ranging from 0.88 for the top singlet's 32-strip panel to 0.97 for both of the middle singlet's panels. An efficiency of 0.95 is desirable for eventually achieving physics results in the ATLAS Experiment's cavern. [43]

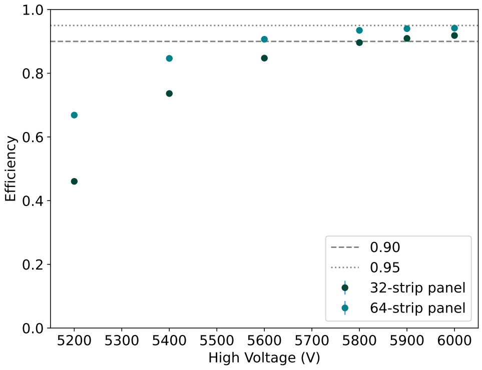


**(a)** Bottom singlet

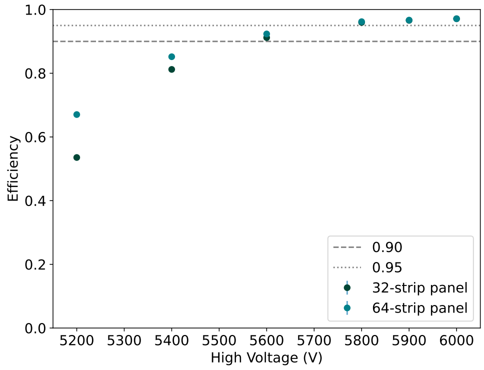


**(b)** Middle singlet

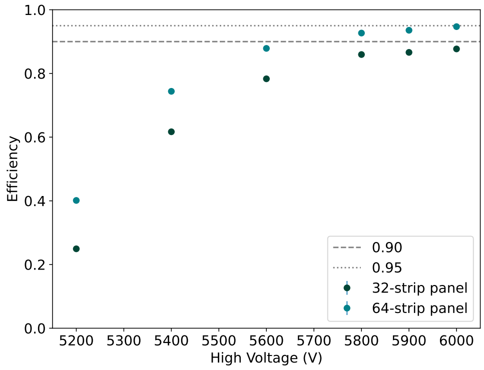


**(c)** Top singlet

**Figure 3.6:** Efficiencies of the singlets of one of proANUBIS' triplets, with benchmarks for 0.90 and 0.95 marked. Uncertainties are given by $1\sigma$ of the Clopper-Pearson interval, though they are too small to be perceptible in these plots.

Figure 3.6b shows that the efficiency of the middle singlet has been measured to be considerably higher than that of its neighboring singlets. This result may, however, be spurious. During data collection, the cables supplying high voltage to the gas gaps were fitted with filters in order to reduce the amount of noise that they produced. After collecting the data used for the analysis shown in figure 3.6, it was found that the filter on the line supplying the middle singlet was faulty. During that run of data collection, the middle singlet registered considerably higher occupancy than its neighbors, likely indicating a considerably higher noise rate. This manifested in an artificially higher measured efficiency of the singlet, and an artificially lower efficiency of its neighbors. With many noise hits, the middle singlet may have often been found to have a coincidence with adjacent singlets when it wouldn't have otherwise registered a signal, increasing its measured efficiency. Conversely, the singlet would have been more likely to create fake coincidences with another singlet's noise hits, which

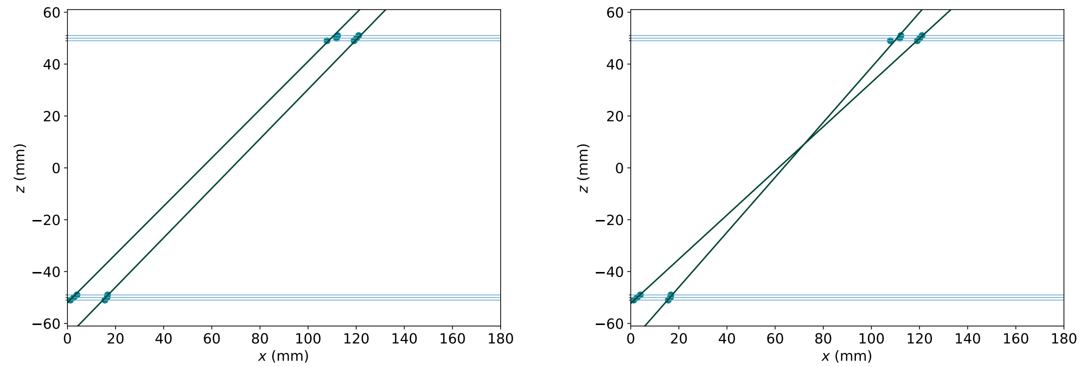


**(a)** Correct reconstruction

**(b)** Incorrect reconstruction

**Figure 3.7:** Reconstructed tracks from two simulated particles passing through one dimension of proANUBIS using (a) the correct hits for each track and (b) the incorrect hits for each track. Positions of RPC singlets in a symmetric configuration shown by light blue lines.

then decreased the measured efficiency of the third singlet where a coincidence should not have been observed. More data with a proper noise filter is therefore necessary in order to fully understand this triplet's performance and compare it to the desired benchmarks for physics results. Efficiency measurements must also be taken for proANUBIS' other triplet.

## 3.4 proANUBIS Layout

Once both triplets have been commissioned, they will be installed to proANUBIS' mechanical frame. This frame will arrange the two triplets 100 cm apart, emulating one of ANUBIS' tracking stations, however it has been decided that one of the triplets' singlets will be offset. One singlet will be placed halfway between the triplet's other two singlets and the other triplet. There will therefore be 50 cm between the singlet and a triplet, and 50 cm between the singlet and a doublet. This has been found in simulations to aid in track disambiguation, which refers to the separation of two tracks which pass nearby one another. Should two adjacent particles pass through proANUBIS in the same event, imprecision of the detector could cause the wrong trajectories to be reconstructed. An example of this can be seen in figure 3.7 where two simulated tracks are observed by proANUBIS in one dimension with a symmetric configuration of RPC singlets (two triplets). Each hit has been smeared by a Gaussian distribution whose standard deviation is the projected uncertainty of a hit registered by a BIS78 RPC with 25 mm pitch ($\approx$ 7.2 mm).[32] In figure 3.7a, the correct tracks

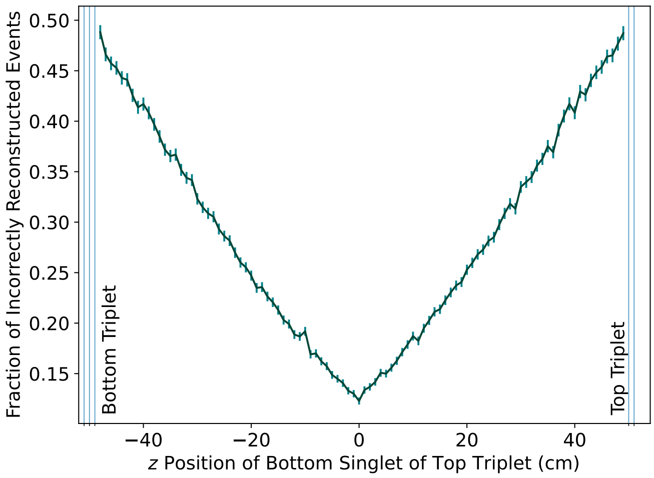


**Figure 3.8:** Fraction of events in which adjacent tracks are incorrectly reconstructed, shown for each possible placement of one proANUBIS singlet between its adjacent singlets. Uncertainties given by taking the square root of the number of incorrectly reconstructed events to estimate $1\sigma$ of the Monte Carlo statistics.

have been reconstructed, however in 3.7b, the tracks have been fit using the incorrect clusters of hits; that is, using the bottom three hits of one particle's trajectory, and the top three hits of the other particle's trajectory, and vice versa. Clearly, this yields very different fits. Smearing of individual hits due to the detector's imprecision could cause these incorrectly reconstructed tracks to be selected over the correct ones if the incorrect tracks are found to be better fits to the perturbed data than the correct ones. Simulations show that this occurrence is least likely when one singlet is placed halfway in-between the other RPC layers.

This simulation is carried out using a Monte Carlo method. The simulation analyzes each possible placement of one of proANUBIS' singlets, ranging from 1 cm above the top singlet of the bottom triplet to 1 cm below the bottom singlet of the top triplet, with 1 cm gradations. For each possible configuration, $10^4$ events are generated where each event contains two particles passing through proANUBIS' fiducial region 25 mm (one strip pitch) apart from each other. Hit positions are calculated as the intersection points of the particles with proANUBIS' singlets, then they are smeared by a Gaussian whose standard deviation is set to the aforementioned singlet precision. Two straight-line tracks are then fit to the six known hits of each particle's trajectory, and the $\chi^2$ goodness-of-fit metric is calculated for both of these fits. Two different straight-line tracks are then fit, this time swapping the hits used above the detector's midpoint. Typically, this means fitting to the three leftmost hits on the detector's bottom half and the three rightmost hits on the detector's top half, and vice versa; this therefore represents an extreme case of incorrect reconstruction, such as what is shown in figure 3.7b. The $\chi^2$ goodness-of-fit of these two tracks to the hits is then calculated again. If the average $\chi^2$ of the two incorrectly reconstructed tracks is found to be lower than that of the two correctly reconstructed tracks, then the event is considered to be incorrectly reconstructed.

Figure 3.8 shows the result of this simulation. Clearly, adjacent tracks are incorrectly reconstructed with the highest frequency when the middle singlet is placed directly next to the detector's other singlets. Events are incorrectly reconstructed with the lowest frequency when the middle singlet is placed halfway between its neighboring singlets. This matches intuition as it adds a data point with a large lever arm between existing readouts from other singlets. For this reason, proANUBIS' frame, designed by Prof. Christopher Lester, has been constructed so that one singlet can be held in the middle of the detector. Given that the detector will collect data at a rather large distance from the interaction point, it is possible that many particles from secondary interactions or punch-through jets will traverse the detector close and nearly parallel to one another. This singlet configuration should then give proANUBIS the best ability to resolve these scenarios.

Once all of the RPC detectors have been commissioned and installed to proANUBIS' frame, proANUBIS will be placed on the surface above the PX14 service shaft, as shown in figure 3.9. Here, it will measure the flux of the particles which pass through the concrete shielding installed on top of the shaft, and provide a useful measurement of the attenuation provided by these beams. Once the cavern becomes accessible during an upcoming shutdown, likely in 2023, proANUBIS will then be moved underground to its final location in the ATLAS Experiment's cavern, also shown in figure 3.9. There, it will measure the flux of particles from punch-through jets which pass through the ATLAS Experiment's calorimeter, and from secondary interactions. This will provide an important measurement of the rate of background with which ANUBIS will have to contend, therefore helping to validate simulations of the events in this region. This pursuit is therefore vital for advancing the ANUBIS project.

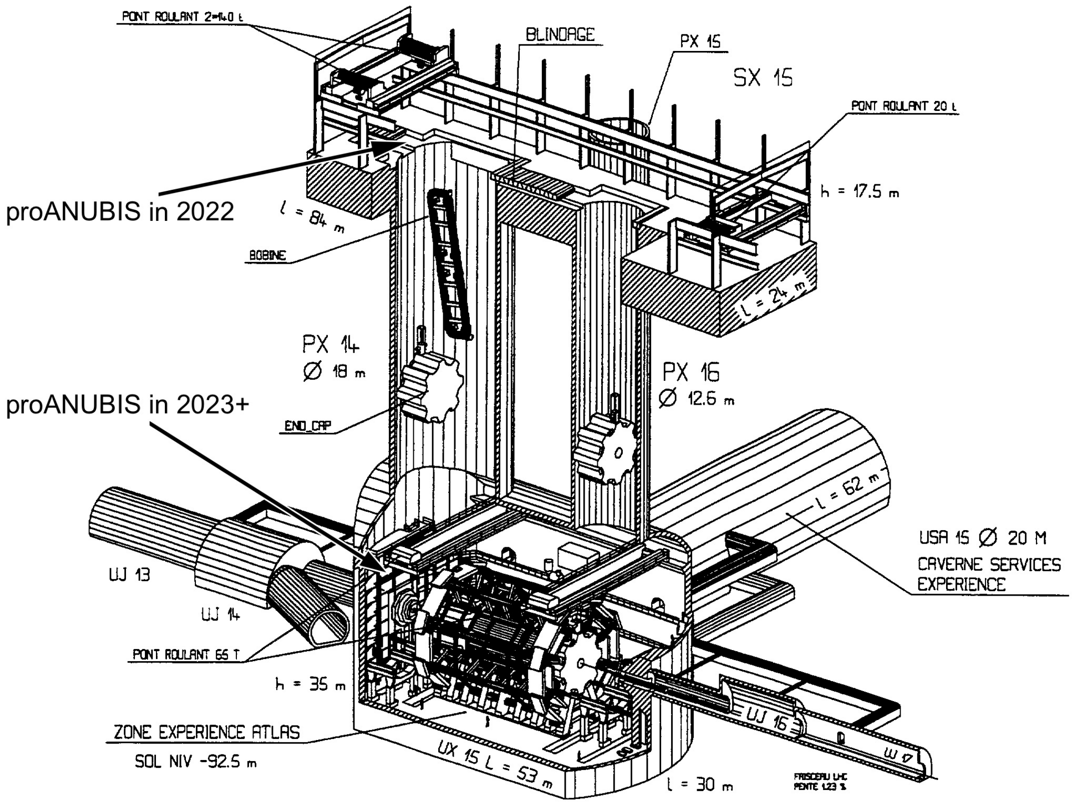


**Figure 3.9:** Schematic of the ATLAS Experiment's cavern and service shafts showing the positions of proANUBIS during Run 3 of data collection at the LHC. Note that several items are shown in the service shafts as a demonstration of how material is transported through them. Source: CERN.[20]

# 4

# Studies of Signal Particles

To understand ANUBIS' viability, this analysis first considers its ability to observe signal: the decays of BSM neutral LLPs. One main benchmark model for this process has been identified, which is the decay of a Higgs boson into a pair of neutral BSM LLPs, which each decay into a $b\bar{b}$ pair. These quarks then hadronize, producing final state, charged jet particles which could be observed by one or more of ANUBIS' tracking stations. This model has been constructed using two modes of Higgs production: gluon fusion (ggF) and vector boson fusion (VBF), as these are the dominant processes with cross sections of 54.7 and 4.28 pb at $\sqrt{s} = 14$ TeV, respectively, therefore representing 95% of Higgs production.[102] Feynman diagrams of these processes are shown in figure 4.1. Exotic Higgs decays are considered because this is a common characteristic of BSM theories, including supersymmetry, and decays into $b\bar{b}$ are considered because the LLP would be expected to have Higgs-like Yukawa coupling, making decays into heavy fermions likely.[76 59] This model is sufficiently generic in order to study ANUBIS' sensitivity to a broad range of BSM models, which often predict displaced jets which are similar to those considered in this analysis. It is also consistent

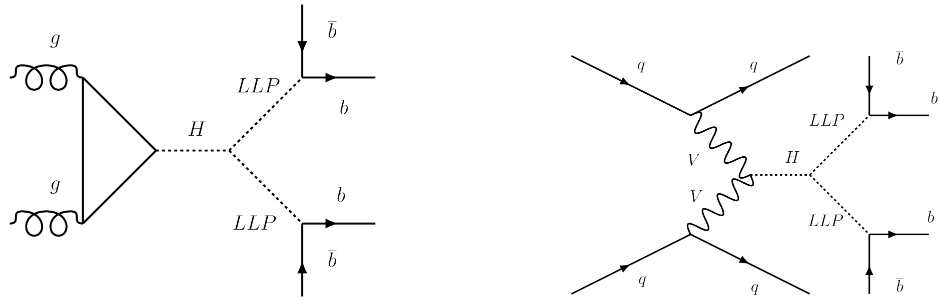


**(a)** ggF

**(b)** VBF

**Figure 4.1:** Feynman diagrams for the two LLP production mechanisms which have been considered in this analysis.

with what has been searched for using the ATLAS and CMS Experiments.[76]

## 4.1 Monte Carlo Simulation

A data set of simulated LLP production and decay has been generated in PYTHIA 8 using code developed in collaboration with Dr. Jonathan Burr.[95, 50] Les Houches event files of Monte Carlo Higgs production in both the ggF and VBF production modes were provided by the ATLAS Experiment. These files, enumerated in table 4.1, were generated using matrix calculations produced by PYTHIA 8 (ggF) and PowHeg (ggF and VBF).[85, 65, 10] PYTHIA 8 is then used to force each Higgs boson to decay into a pair of invisible, Higgs-like LLPs (PDG ID 35), with masses of 10, 20, 30, or 40 GeV.[102] These LLPs are forced to decay into $b\bar{b}$ pairs before hadronizing. This generates a suitable data set from which the final state, charged jet particles of a BSM LLP decay can be studied in order to understand the sensitivity of ANUBIS to this model. Table 4.2 lists the number of LLPs which are generated for each Higgs production mechanism and each LLP mass. In total, nearly $10^8$ LLPs are simulated for each mass point.

This data set is augmented slightly in order to increase the number of simulated observations of LLP decays by ANUBIS. LLPs whose $\varphi$ coordinate points downwards (away from ANUBIS' tracking stations) are unlikely to be detected by the experiment. A number of backwards-going jet particles in an event could perhaps be detected by ANUBIS' tracking stations, however this is likely to be an exceedingly rare occurrence. Therefore, in order to maximize statistics, the data is scaled such that the $\varphi$ coordinate of all LLPs points upwards; for each downward-travelling LLP, a factor

| ggF |
| --- |
| mc15_13TeV.343981.PowhegPythia8EvtGen_NNLOPS_nnlo_30_ggH125_gamgam.evgen.TXT.e5607_tid10248297_00 |
| mc15_13TeV.343981.PowhegPythia8EvtGen_NNLOPS_nnlo_30_ggH125_gamgam.evgen.TXT.e5607_tid10265946_00 |
| mc15_13TeV.343981.PowhegPythia8EvtGen_NNLOPS_nnlo_30_ggH125_gamgam.evgen.TXT.e5607_tid11816472_00 |
| mc15_13TeV.343981.PowhegPythia8EvtGen_NNLOPS_nnlo_30_ggH125_gamgam.evgen.TXT.e5607_tid15522089_00 |
| mc15_13TeV.343981.PowhegPythia8EvtGen_NNLOPS_nnlo_30_ggH125_gamgam.evgen.TXT.e5607_tid13720161_00 |
| mc15_13TeV.343981.PowhegPythia8EvtGen_NNLOPS_nnlo_30_ggH125_gamgam.evgen.TXT.e5607_tid14277219_00 |
| **VBF** |
| mc15_13TeV.345916.Powheg_NNPDF30_VBFH125_LHE.evgen.TXT.e6901_tid15303714_00 |
| mc15_13TeV.345916.Powheg_NNPDF30_VBFH125_LHE.evgen.TXT.e6901_tid15303723_00 |
| mc15_13TeV.345916.Powheg_NNPDF30_VBFH125_LHE.evgen.TXT.e6901_tid15303735_00 |

**Table 4.1:** Monte Carlo data sets used to generate LLP production and decay simulation. Files provided by the ATLAS Experiment.

| Higgs Production Mechanism | LLP Mass (GeV) | Number of LLPs |
| --- | --- | --- |
| ggF | 10 | 76444000 |
| ggF | 20 | 75944000 |
| ggF | 30 | 76112000 |
| ggF | 40 | 76104000 |
| VBF | 10 | 17976000 |
| VBF | 20 | 17916000 |
| VBF | 30 | 17876000 |
| VBF | 40 | 17996000 |

**Table 4.2:** Number of BSM LLPs simulated at each mass point for signal studies. Uses data sets listed in table 4.1.

of $\pi$ is added to its $\varphi$ coordinate, and to the $\varphi$ coordinate of the jet particles that its decay produces. The final number of observed decays is then weighted by a factor of $1/2$, exploiting the symmetry of physics around the ATLAS Experiment's $\varphi$ coordinate to correct for this scaling.

## 4.2 Event Selection

The first step of the data analysis pipeline involves applying a series of event-level cuts. These cuts are aimed at discriminating against background processes, and their merit in background reduction is discussed in section 5. To begin, a cut on the missing energy in the transverse direction ($E_T^{\text{miss}}$) present in the event is applied. In simulation, this quantity is determined by summing the energies of the final state particles which are not observed by the ATLAS Experiment's simulated detectors.

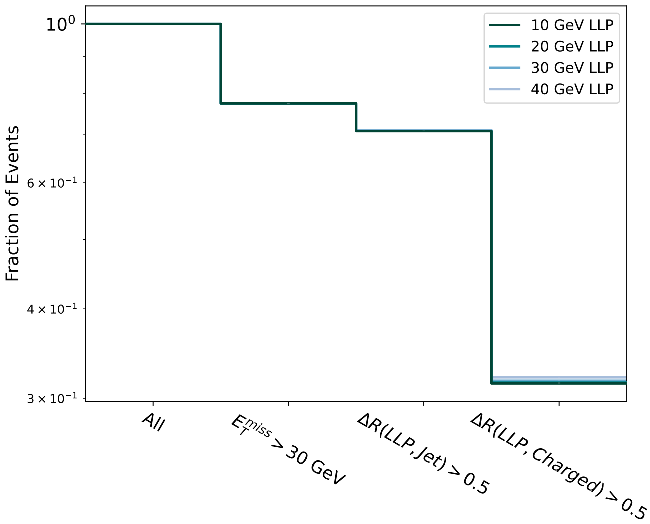


**Figure 4.2:** Cutflow showing the effects of cuts on the presence of $E_T^{\text{miss}}$ and on LLP isolation on the set of simulated BSM LLPs with masses of 10, 20, 30, and 40 GeV. Uncertainties are given by taking the square root of the number of events in each bin to estimate $1\sigma$ of Monte Carlo statistics, though they are too small to be perceptible in this plot.

Experimentally, this is calculated by summing the observed energies, in the *xy*-plane, of the particles which are detected in a *pp* collision. These energies should sum to zero by the conservation of energy, so a nonzero value indicates one or more particles which escaped detection.[22] This cut is applied as it is likely to be a characteristic signal of neutral BSM LLPs which traverse a particle detector without observation.[76] Therefore, an event is required to have $E_T^{\text{miss}} > 30$ GeV as this cut has been found to significantly reduce background while still preserving a suitable amount of signal.

Two isolation cuts are also applied to the trajectories of reconstructed LLPs. In simulation, this is achieved by considering the truth-level trajectories of BSM LLPs, Standard Model jets, and charged particles. In practice, this is accomplished using the reconstructed trajectories of these particles. LLPs are required to be sufficiently isolated from nearby jets and charged particles as these occurrences are indicative of the production of background events.[24] This is accomplished by calculating the quantity $\Delta R \equiv \sqrt{(\Delta\eta)^2 + (\Delta\varphi)^2}$ and requiring that it is in excess of 0.5 for each LLP when paired with all nearby jets and charged particles in the same event. As with the cut on $E_T^{\text{miss}}$, this has been found to reduce background while still maintaining a suitable level of signal. The effects of these cuts on the simulated LLP-producing events are shown in figure 4.2. This shows that on the order of 30% of signal events are preserved following the application of these cuts.

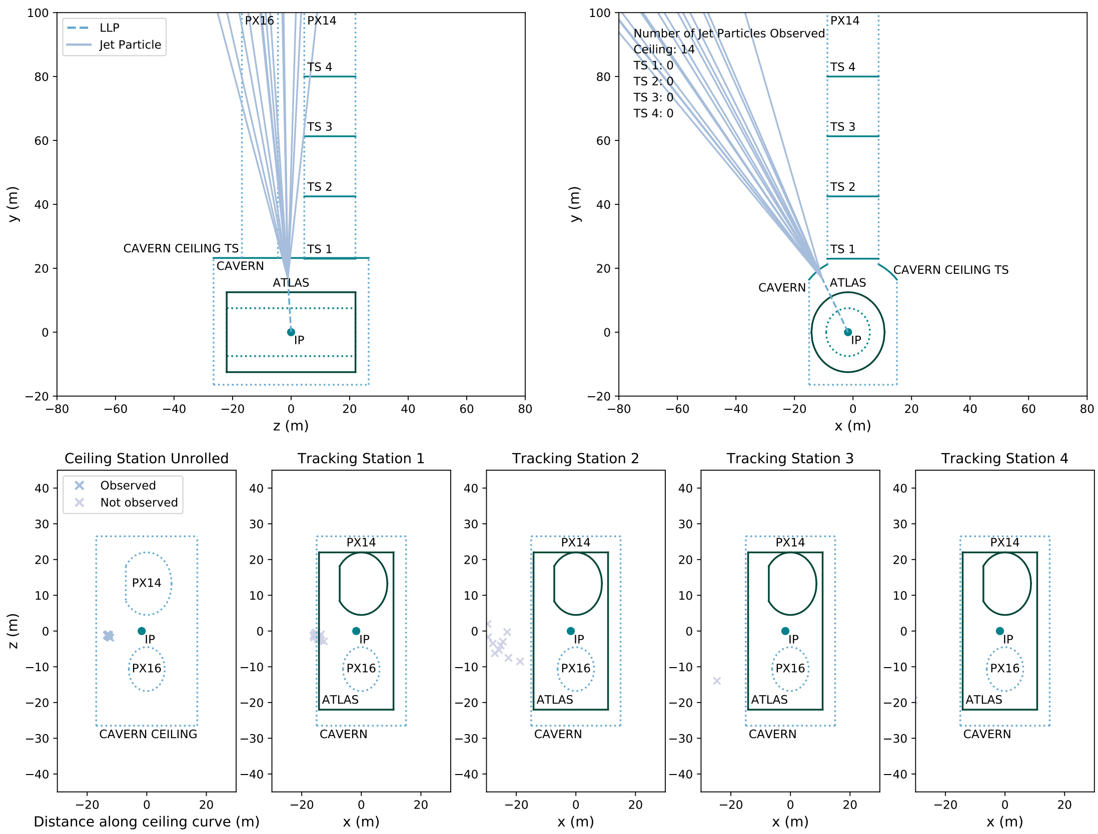


**Figure 4.3:** Event display showing how an in-cavern decay of a 10 GeV LLP could be observed by ANUBIS in the ceiling configuration, but not in the in-shaft configuration. Trajectories of the LLP and ensuing jet particles are shown by dashed and solid lines, respectively. As shown, 14 final state, charged jet particles would be observed by ANUBIS' ceiling tracking station (TS), with no other tracking stations registering observations in this event. Top row shows a cross sections of the ATLAS Experiment's cavern and service shafts in the $zy$- (left) and $xy$- (right) planes. Dotted lines indicate the extent of the ATLAS Experiment's vertexing limit, shown within the solid lines of its physical extent. Bottom row shows intersection positions of final state, charged jet particles with ANUBIS' various proposed tracking stations. Note that the bottom-left figure is in local (curved) coordinates of the ceiling tracking station.

## 4.3 Geometric Model

The data analysis pipeline then considers how many LLP-producing events which pass these cuts have final state, charged jet particles which intersect ANUBIS' tracking stations. Jet particles are required to have a momentum in excess of 100 MeV as this would likely be necessary for detection by BIS78 RPC detectors. Furthermore, any jet particle which passes through concrete or earth before intersecting a tracking station is not considered as these would likely be absorbed by the material. A LLP is required to produce at least two particles which intersect at least one of ANUBIS' tracking

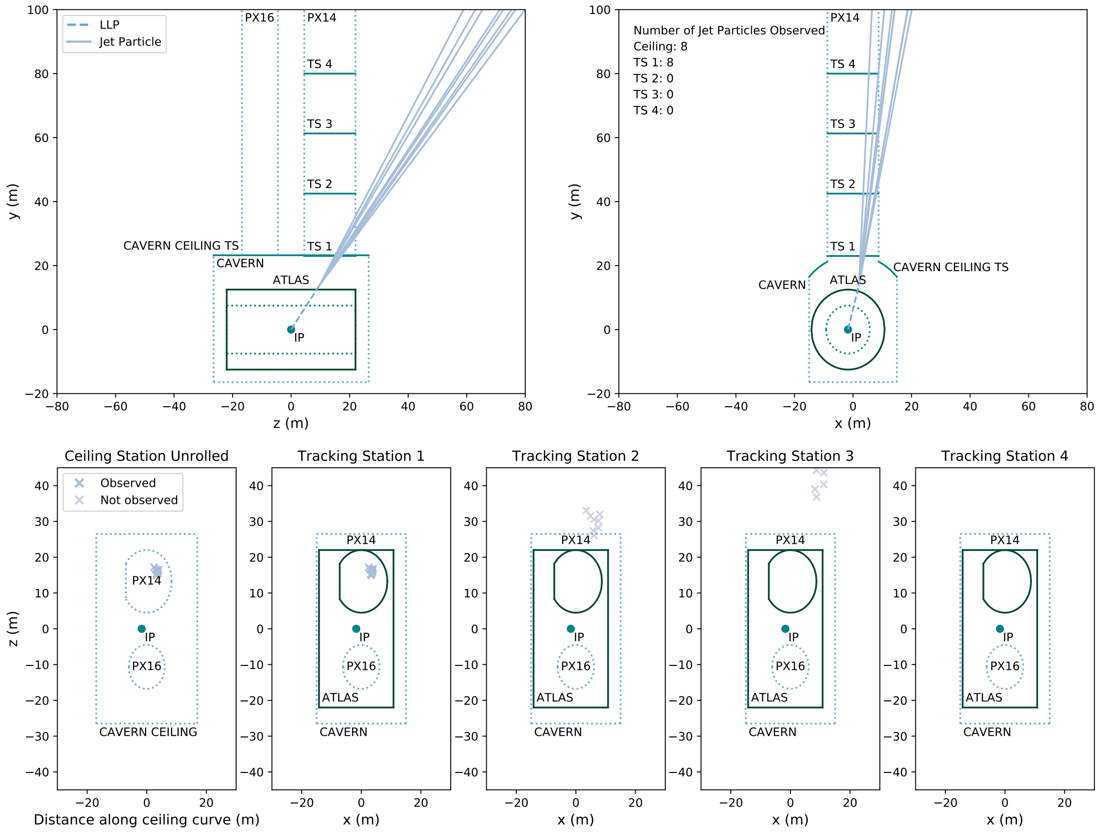


**Figure 4.4:** Event display showing how an in-cavern decay of a 10 GeV LLP could be observed by ANUBIS in the ceiling and shaft configurations. Uses the same format as what is described in the caption of figure 4.3. As shown, 8 final state, charged jet particles would be observed by ANUBIS' ceiling tracking station and first in-shaft tracking station.

stations in order for the event to be considered observed as this would produce the minimum information necessary to reconstruct the parent LLP's vertex. This does not consider the probability that a charged jet particle of sufficient momentum evades detection by a tracking station as the relatively high efficiency of the BIS78 RPC technology makes this scenario unlikely.[32] For simplicity, the LLP is considered to be produced precisely at the ATLAS Experiment's interaction point, and its final state particles are considered to be produced precisely at the LLP's vertex. These assumptions are justified given the short lifetimes of the LLP's progenitor, the Higgs boson, and of the intermediate jet particles that the LLP produces, meaning that they would have little effect on the final outcome of this analysis.[102]

Two scenarios for LLP decays and subsequent observations are considered. The in-cavern sce-

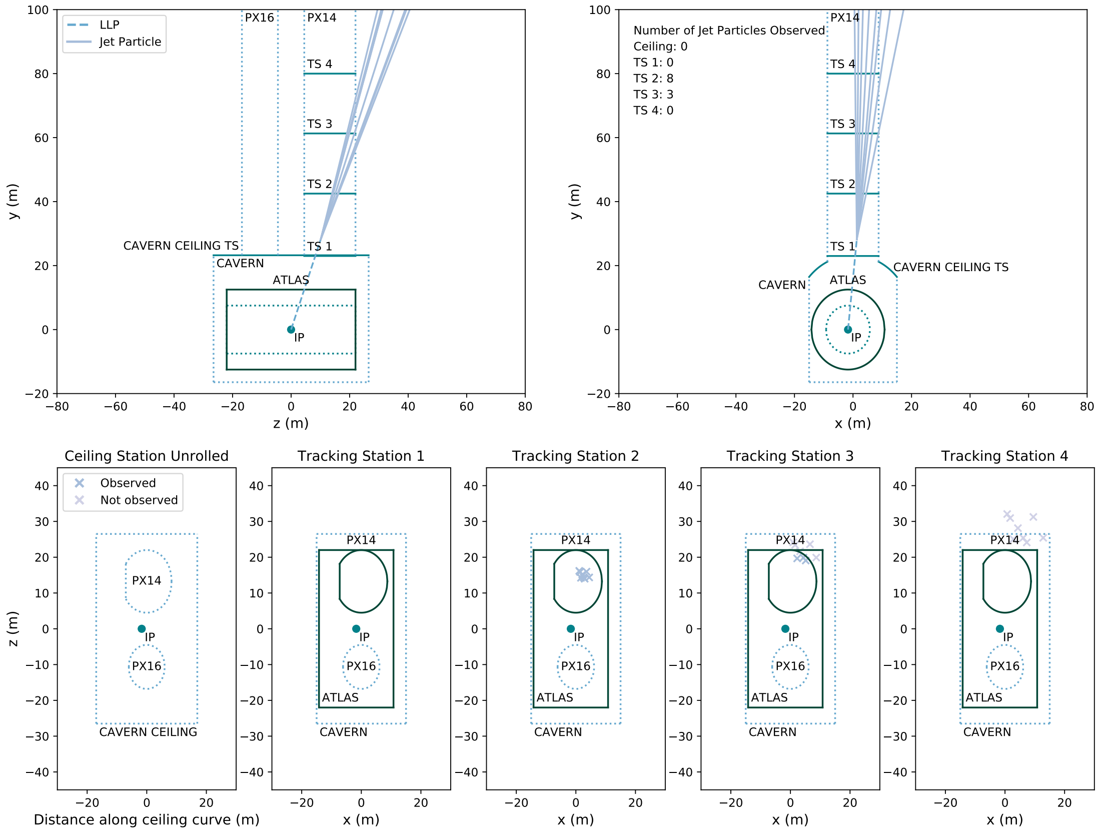


**Figure 4.5:** Event display showing how an in-shaft decay of a 10 GeV LLP could be observed by ANUBIS in the shaft configuration, but not in the ceiling configuration. Uses the same format as what is described in the caption of figure 4.3. As shown, 8 final state, charged jet particles would be observed by ANUBIS' second in-shaft tracking station, and 3 would be observied by its third. None would be observed by its first or fourth in-shaft tracking stations.

nario searches for LLPs which decay anywhere between the ATLAS Experiment's vertexing limit ($r = 7.5$ m from the beamline) and the bounds of its cavern.[3] This scenario could be observed by either the ceiling or the PX14 shaft configurations of ANUBIS, and it assumes that the ATLAS Experiment can be used to sufficiently discriminate against background. The in-shaft scenario searches for LLPs which decay within the PX14 service shaft, anywhere after ANUBIS' first PX14 shaft tracking station. Only the PX14 shaft configuration of ANUBIS would therefore be sensitive to this scenario of decays, however it would allow for the first tracking station to aid in background discrimination.[43] Examples of in-cavern decays are shown in figures 4.3 (ceiling configuration) and 4.4 (cavern and shaft configuration), and an example of an in-shaft decay is shown in figure 4.5. These event displays were generated using the code whose results I present in this thesis. Note that in both scenarios, jet particles are assumed to not be affected by the ATLAS Experiment's magnetic field. This assumption is justified by the fact that the field is largely confined to the ATLAS Experiment's physical bounds, so any resulting perturbation of jet particles from leakage outside of this region would be of a small magnitude, and it would likely occur equally in all directions. [16] This would therefore yield a negligible effect on the final sensitivity.

## 4.4 Sensitivity

For the entire data set of BSM LLP productions and decays, each event is considered by this geometric model for a given proper lifetime ($\tau$) of the LLP. Given a LLP and a value of $\tau$, an exponential distribution whose scale factor is $c\tau$ times the particle's relativistic boost $\gamma = \sqrt{p^2 + m^2}/m$ for mass $m$ and momentum $p$ and its $\beta = v/c$ for velocity $v$ is sampled in order to determine how far the particle travels in the lab frame before decaying. The distribution for decay distance $x$ is therefore given by the probability density function:

$$\mathrm{P}(x) = \frac{1}{\gamma\beta c\tau} e^{-x/(\gamma\beta c\tau)}$$

This analysis considers values of $c\tau$ ranging from $10^{-3}$ m to $10^{8}$ m with values probed every fifth of an order of magnitude. These bounds are considered as they have been found to form the limits of ANUBIS' sensitivity.

Given a certain number of observations, $N_{\text{obs}}$, in a total data set of $N_{\text{tot}}$ LLP productions and decays for fixed $\tau$, we can consider ANUBIS' acceptance times its efficiency in a given scenario and configuration to be the ratio of these quantities. In order to observe a certain number of LLP decays, $N_{\text{LLP}}$, at HL-LHC conditions, given by integrated luminosity $\mathcal{L}_{\text{HL-LHC}}$ and Higgs production cross section $\sigma_{\text{Higgs}}$, then these LLPs must be produced with branching ratio $\text{Br}(H \to \text{ss})$ given by:

$$N_{\text{LLP}} = \mathcal{L}_{\text{HL-LHC}} \cdot \sigma_{\text{Higgs}} \cdot 2 \cdot \text{Br}(H \to \text{ss}) \cdot \frac{N_{\text{obs}}}{N_{\text{tot}}} \tag{4.1}$$

This equation is then used to determine to which branching ratios of BSM LLP production ANUBIS would be sensitive enough to observe a certain number of LLP decays during the 3 $\text{ab}^{-1}$ of data which are expected to be produced by the HL-LHC. [14]

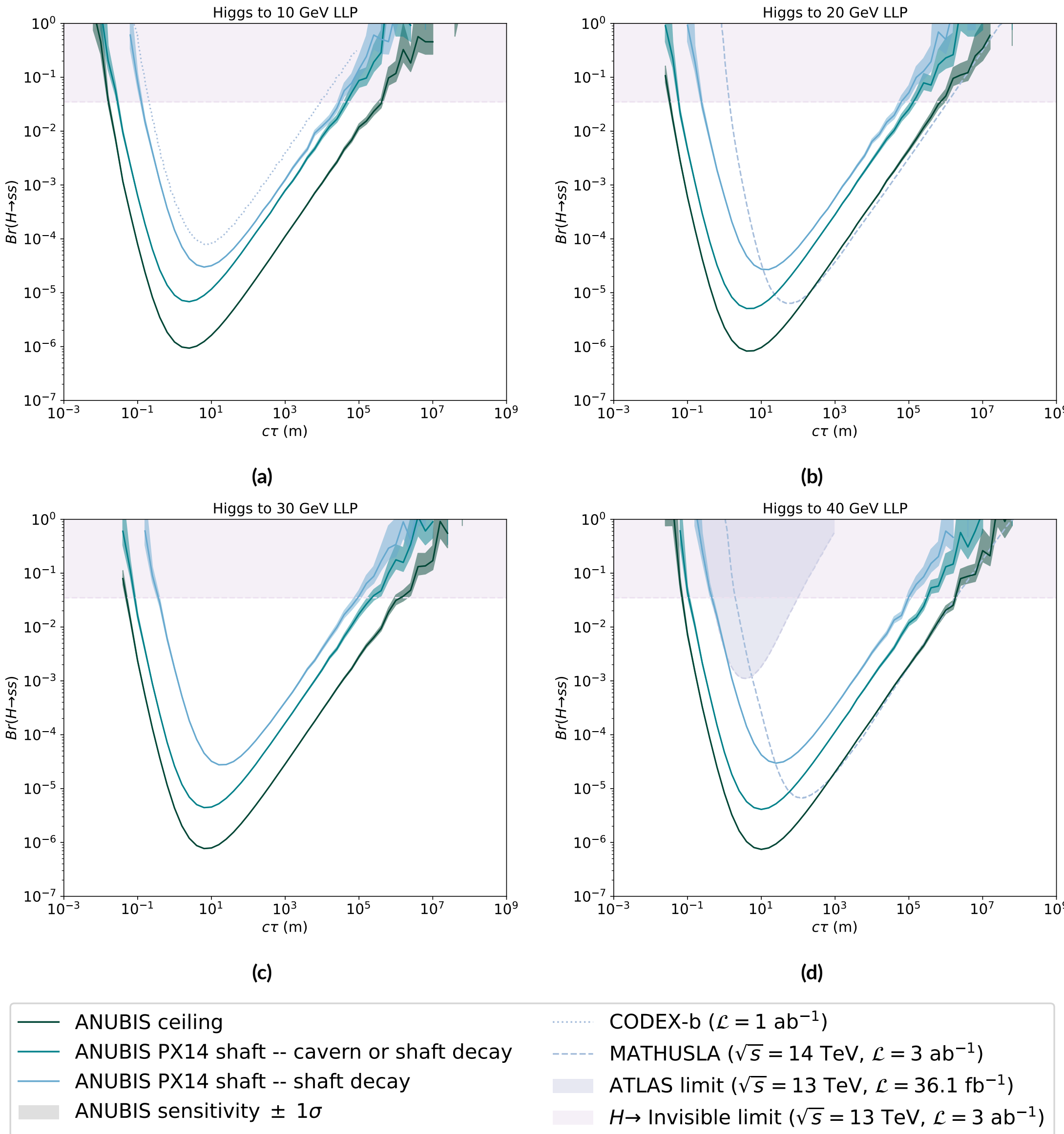


**Figure 4.6:** Branching ratio sensitivity of ANUBIS' various configurations to four observations of the decays of Higgs portal BSM LLPs with masses of (a) 10, (b) 20, (c) 30, and (d) 40 GeV at HL-LHC conditions ($\sqrt{s} = 14$ TeV, $\mathcal{L} = 3\,\text{ab}^{-1}$). Uncertainties given by Monte Carlo statistics. Compared to a result from the ATLAS Experiment which searched for 40 GeV BSM LLPs, and available projections for CODEX-b searching for 10 GeV BSM LLPs and MATHUSLA searching for 20 and 40 GeV BSM LLPs, as well as the projected limit for decays of the Higgs boson into invisible particles at the HL-LHC.[3 67 55 45]

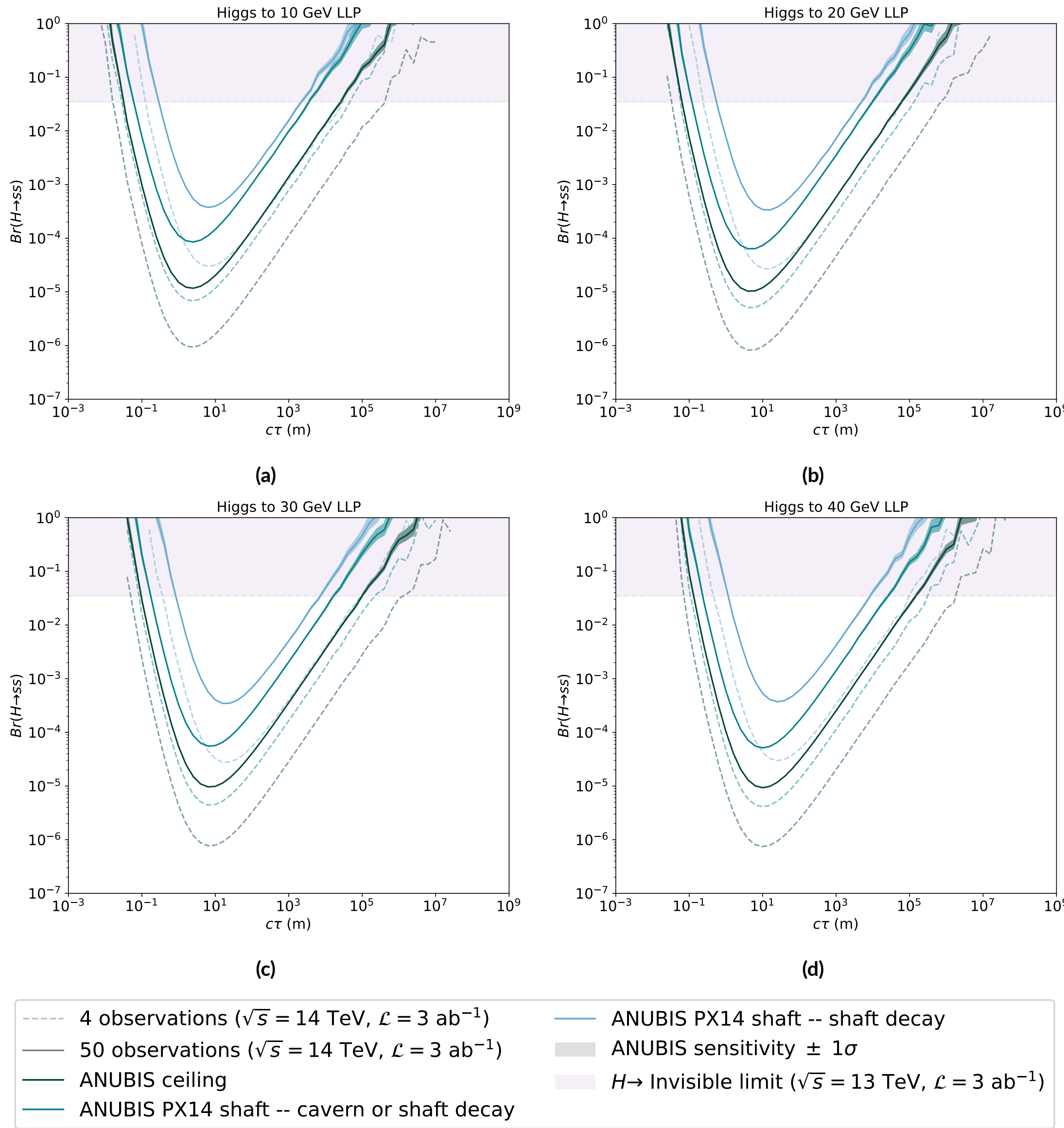


**Figure 4.7:** Branching ratio sensitivity of ANUBIS' various configurations to fifty observations of the decays of Higgs portal BSM LLPs with masses of (a) 10, (b) 20, (c) 30, and (d) 40 GeV at HL-LHC conditions. Compared to its sensitivity to four such decays, as given in figure 4.6, as well as to the projected limit for decays of the Higgs boson into invisible particles at the HL-LHC.[45]

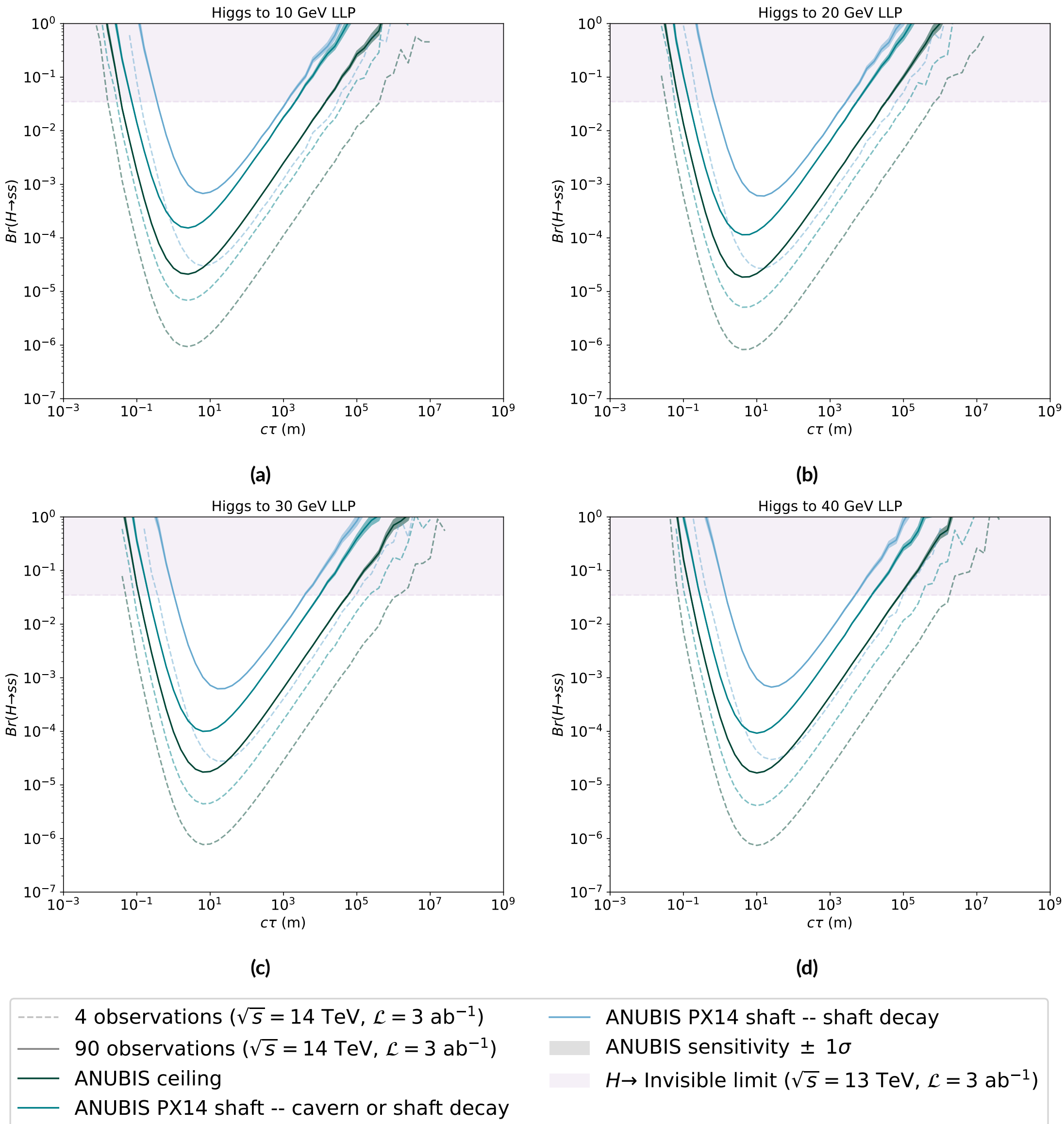


**Figure 4.8:** Branching ratio sensitivity of ANUBIS' various configurations to ninety observations of the decays of Higgs portal BSM LLPs with masses of (a) 10, (b) 20, (c) 30, and (d) 40 GeV at HL-LHC conditions. Compared to its sensitivity to four such decays, as given in figure 4.6, as well as to the projected limit for decays of the Higgs boson into invisible particles at the HL-LHC.[45]

## 4.5 Results

Assuming that ANUBIS is a background-free experiment, four observations would represent a significant deviation from the expectation over the course the HL-LHC's operation, therefore providing compelling evidence for BSM LLPs.[43] In the presence of moderate background, fifty observations may be necessary in order to claim a significant result using the shaft configuration of ANUBIS. This follows from a recent result from the ATLAS Experiment which searched for BSM LLPs using the experiment's muon spectrometer, which lies roughly below the PX14 service shaft, and observed a similar number of background events.[3 43] This quantity can be scaled to the ceiling configuration by considering the square root of the ratio of the relevant decay volumes, assuming that the uncertainty on background is largely statistical. This calculation is discussed in appendix A, and it leads to a requirement of $50 \cdot \sqrt{3.2} \approx 90$ observations. For these benchmarks, it is only necessary that one of the pair-produced LLPs is observed by ANUBIS while the other is assumed to decay somewhere outside of the ATLAS Experiment; otherwise the search would be free of background.

Results for the branching ratios of LLP-production to which ANUBIS would be sensitive enough at HL-LHC conditions to observe four observations are shown in figure 4.6. Uncertainty is given by taking $N_{\text{obs}} \rightarrow N_{\text{obs}} \pm \sqrt{N_{\text{obs}}}$ and propagating this through equation 4.1 to estimate the statistical uncertainty on branching ratio sensitivity. These results are contrasted with an existing result from the ATLAS Collaboration, as well as similar projections for Higgs-portal BSM LLP searches at CODEX-b and MATHUSLA in the same figure.[3 67 55] Figure 4.7 compares these results to a similar analysis which searches for fifty observations rather than four, and figure 4.8 shows the results for a search for ninety events. Note that in all figures, odd behavior can be seen in the high-$c\tau$ region, especially in figures 4.6d, 4.7d, and 4.8d. This is likely a statistical fluctuation due to the low number of events which intersect ANUBIS given this lifetime, however it is within the excluded region for the branching ratio of the Higgs boson to invisible particles, meaning that ANUBIS' sensitivity is irrelevant.

These results show exciting potential for the ANUBIS project. For each mass point, the sensitivity peaks at branching ratios reaching $\mathcal{O}(10^{-6})$. This is achieved when searching for LLPs with $c\tau$ of approximately 3, 4, 6, and 10 m for masses of 10, 20, 30, and 40 GeV, respectively. This sensitivity would be realized by the ceiling configuration of detectors when searching for four observations, and a sensitivity to these particles reaching $\mathcal{O}(10^{-5})$ would be realized when instead searching for ninety observations in the same configuration. At its peak sensitivity, this represents an improvement of two to three orders of magnitude, depending on the goal number of observations, over a recent result from the ATLAS Experiment which searched for a 40 GeV BSM LLP using displaced vertices in its muon spectrometer.[3] These results also show that ANUBIS would be sensitive to a much wider range of proper lifetimes than the search from the ATLAS Experiment, showing sensitivity for $c\tau$ ranging from about $10^{-1}$ to $10^{5}$ m when searching for ninety events before reaching the limit for Higgs decays into invisible particles. At the upper end, this is within two orders of magnitude of the limit provided by Big Bang nucleosynthesis.[64] The in-shaft configuration also shows exciting promise, with sensitivity shifted to branching ratios about three quarters of an order of magnitude higher than those of the ceiling configuration. For in-shaft decays only, peak sensitivity is again raised by about three quarters of an order of magnitude, though it is also shifted towards slightly higher values of $c\tau$. When searching for four events, this projects sensitivity to branching ratios of $\mathcal{O}(10^{-5})$ for 10, 20, 30, and 40 GeV particles with $c\tau$ of approximately 6, 16, 16, and 25 m, respectively. This sensitivity is raised by an order of magnitude when instead searching for 50 events, though it still shows significant improvement over the sensitivity of the ATLAS Experiment alone.

The improvement of the ceiling configuration over the shaft configuration of ANUBIS elucidates an important point in searching for LLPs: increased solid angle coverage close to the interaction point can outweigh reduced solid angle coverage further away from the interaction point. Physics is expected to be symmetric around the ATLAS Experiment's $\varphi$ coordinate, so coverage in twice as much of this coordinate should yield twice as much acceptance. Particle decay, however, follows an exponential distribution.[69] Therefore, depending on the proper lifetime of the particle, doubling the distance from the interaction point to the detector may not double its acceptance. Figure 4.6 shows that the ceiling configuration, whose detectors are considerably closer to the interaction point than the shaft configuration's furthest detectors, but cover a larger solid angle, is more sensitive to LLP decays at all simulated proper lifetimes. This effect is also shown by the curves for in-cavern or in-shaft decays compared to those for in-shaft decays only. The latter is shifted to the right when compared to the former, showing that it reaches similar sensitivity for very long-lived par-

| Mass<br>$c\tau$ | 10 GeV<br>3 m | 10 GeV<br>100 m | 40 GeV<br>10 m | 40 GeV<br>100 m |
|---|---|---|---|---|
| ATLAS Experiment | – | – | $1.9 \times 10^{-3}$ | $3.7 \times 10^{-2}$ |
| CODEX-b | $1.2 \times 10^{-4}$ | $4.2 \times 10^{-4}$ | – | – |
| MATHUSLA | – | – | $2.6 \times 10^{-4}$ | $6.9 \times 10^{-6}$ |
| ANUBIS ceiling | $9.4 \times 10^{-7}$ | $1.2 \times 10^{-5}$ | $7.4 \times 10^{-7}$ | $2.4 \times 10^{-6}$ |
| ANUBIS PX14 shaft – cavern or shaft decay | $6.8 \times 10^{-6}$ | $8.3 \times 10^{-5}$ | $4.1 \times 10^{-6}$ | $1.3 \times 10^{-5}$ |
| ANUBIS PX14 shaft – shaft decay | $4.3 \times 10^{-5}$ | $1.4 \times 10^{-4}$ | $4.2 \times 10^{-5}$ | $4.8 \times 10^{-5}$ |

**Table 4.3:** Comparison of ANUBIS' branching ratio sensitivity to four observations of Higgs-portal LLP decays to a result from the ATLAS Experiment and available projections from CODEX-b and MATHUSLA.[3 67 55]

ticles ($c\tau > 10^2$ m), however it is far outpaced for considerably shorter lifetimes ($c\tau < 1$ m) as there are not many of these particles which make it to the PX14 shaft before decaying.

These results also show that ANUBIS is competitive with other proposals to enhance the LHC's experiments in pursuit of BSM LLPs, as shown in table 4.3. ANUBIS' most restrictive scenario, which searches for in-shaft decays, shows sensitivity which improves upon that of CODEX-b by about three quarters of an order of magnitude when searching for four observations of a 10 GeV Higgs-portal LLP with $c\tau$ of 3 m.[67] The project's in-cavern or in-shaft PX14 scenario shows an improvement of more than one order of magnitude when compared to the CODEX-b projection for this LLP model, and its ceiling configuration gives a further improvement of about three quarters of an order of magnitude. When compared to MATHUSLA in the search for four observations of 20 or 40 GeV Higgs-portal LLPs, ANUBIS' peak ceiling configuration sensitivity at $c\tau$ of 4 and 10 m, respectively, shows an improvement of more than two orders of magnitude.[55] MATHUSLA's peak sensitivity is achieved at $c\tau$ of approximately 100 m, and this sensitivity is slightly improved upon by ANUBIS' ceiling configuration. MATHUSLA's increased distance from the interaction point allows it to improve upon ANUBIS' bounds by about a half order of magnitude for longer proper lifetimes however, consequently, ANUBIS significantly improves upon MATHUSLA's sensitivity for shorter proper lifetimes. In the PX14 shaft configuration, ANUBIS shows comparable sensitivity to MATHUSLA for proper lifetimes shifted by about one order of magnitude towards the shorter end. The CODEX-b and MATHUSLA projects do, however, have the added benefits of increased shielding from background due to cavern material and earth existing between the interaction point and their detectors. The background-free assumption which searches for four observations may therefore be more realistic for these proposals than for ANUBIS.

These results show that ANUBIS has exciting potential for detecting BSM LLPs in both of its configurations. It significantly improves upon the ATLAS Experiment's current capabilities, and it shows comparable or better projections than the CODEX-b and MATHUSLA proposals. In order to realize this exciting set of detectors, however, it is necessary to better understand the background processes with which it will have to contend. This pursuit is discussed in the following section.

# 5
# Studies of Background Particles

The ANUBIS project, like any experiment, will have to contend with background events: Standard Model processes whose signatures on its detectors mimic those of BSM LLPs. Understanding the characteristics of these events, as well as their frequencies, therefore forms a vital component of studying ANUBIS' viability. This can be achieved using a similar methodology to what was discussed in section 4 for signal events. After identifying a number of background processes, Monte Carlo simulations can be generated, to which event-level cuts can be applied, and acceptance by ANUBIS' proposed tracking stations can be studied. This has been carried out using a combination of PYTHIA 8 and GEANT4 to generate simulations of neutron and long-lived neutral kaon decays and hadronic interactions with air so that the signals that these events would induce on ANUBIS' tracking stations can be analyzed.

## 5.1 Sources of Background

Neutrons (quark content $udd$) and long-lived neutral kaons (quark content $(d\bar{s}+s\bar{d})/\sqrt{2}$) have been identified as potential sources of background due to their frequent production in $pp$ collisions and their relatively long lifetimes, which would allow them to reach ANUBIS' detectors. Neutrons ($n^0$) have a mean lifetime of 879 s and long-lived neutral kaons ($K^0_L$) have a mean lifetime of $5.12 \times 10^{-8}$ s ($c\tau \approx 15.3$ m).[102] As these particles are both neutral, they could traverse the ATLAS Experiment's detectors without being observed, just as a BSM LLP would, and they could interact beyond these existing detectors and produce a signal in ANUBIS' tracking stations. $n^0$ are not likely to decay on the distance scale of ANUBIS, however they could scatter off of air molecules in the ATLAS Experiment's cavern and generate a jet of particles. $K^0_L$ could decay on the distance scale of ANUBIS' detectors, and they could also interact with air molecules to produce jets.[102] Both types of particle could also interact with detector or cavern material however, for simplicity, this study focuses on interactions with air and whether these events would significantly hinder ANUBIS' ability to discover new, exotic physics.

In order for a $n^0$ or $K^0_L$ to interact with ANUBIS in a way that would mimic a BSM LLP, it would have traversed the ATLAS Experiment without detection or absorption. This would mean that it would not have interacted with detectors, including the calorimeters which serve to attenuate punch-through jets.[16] The ATLAS Experiment's calorimeters measure 9.7 radiation lengths at $\eta = 0$, meaning that the probability of traversal without absorption has a lower bound of $e^{-9.7} \approx 6.1 \times 10^{-5}$.[57] While this would significantly reduce the amount of background which would reach ANUBIS, HL-LHC conditions mean that a significant number of events might still remain. This study therefore seeks to determine how much further attenuation is provided by the event level cuts which were applied to signal particles in the studies presented in section 4, and by requiring the same level of observation by ANUBIS' tracking stations.

## 5.2 Monte Carlo Simulation

The data set for this study is formed using PYTHIA 8 and GEANT4. As before, a data set of $pp$ collisions is produced using PYTHIA 8, however the simulation is not initialized with Les Houches

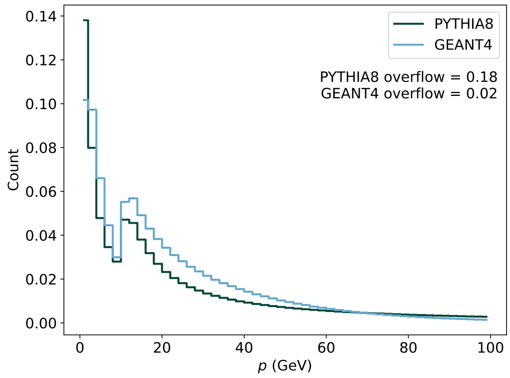


**(a)** $K_L^0$

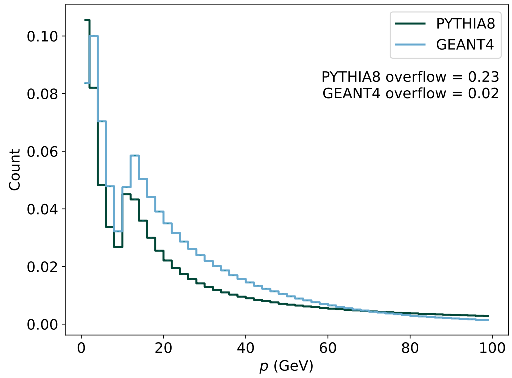


**(b)** $n^0$

**Figure 5.1:** Momentum distributions of simulated (a) $K_L^0$ and (b) $n^0$ generated using PYTHIA 8 and GEANT4. Uncertainties are given by taking the square root of the number of events in each bin to estimate $1\sigma$ of Monte Carlo statistics, though they are too small to be perceptible in this plot.

event files of Higgs production events.[95 50] Instead, PYTHIA 8 simulates the production of a broad spectrum of particles following an inelastic *pp* collision, without bias towards any specific process; this is known as the simulation of "minimum-bias" collisions. Events which involve the production of a $n^0$ or $K_L^0$ are recorded as these are most relevant to this study. In total, $10^{10}$ such events are simulated, leading to the production of about $2.3 \times 10^7$ $n^0$ and about $1.7 \times 10^7$ $K_L^0$. Separately, GEANT4 is used to simulate a set of $n^0$- and $K_L^0$-air interactions.[8 11 12] A beam of $n^0$ and, separately, $K_L^0$ with momentum distributions that model those of the $n^0$ and $K_L^0$ produced by the PYTHIA 8 simulation, respectively, are fired through a cylinder of air measuring 100 m in length. These momentum distributions are formed by fitting the sum of two exponential distributions to the momentum distributions of PYTHIA 8 particles and sampling the GEANT4 particles' momenta from these distributions, which yields the those shown in figure 5.1. For each particle, the final state, charged particles produced in the event are recorded. For either particle, these could be the ensuing jet particles from an interaction with air molecules or, for $K_L^0$, these could be the LLP's decay products. It is also possible that no final state, charged particles are recorded if the parent particle traverses the 100 m without interacting. $10^7$ events of $n^0$- and $K_L^0$- interactions are generated for each particle species. These PYTHIA 8 and GEANT4 data sets were generated by Dr. Jonathan Burr.

These two data sets are then paired with one another. For each $n^0$ or $K_L^0$ generated by PYTHIA 8, a corresponding particle is selected from the GEANT4 data set with a momentum within 50 MeV

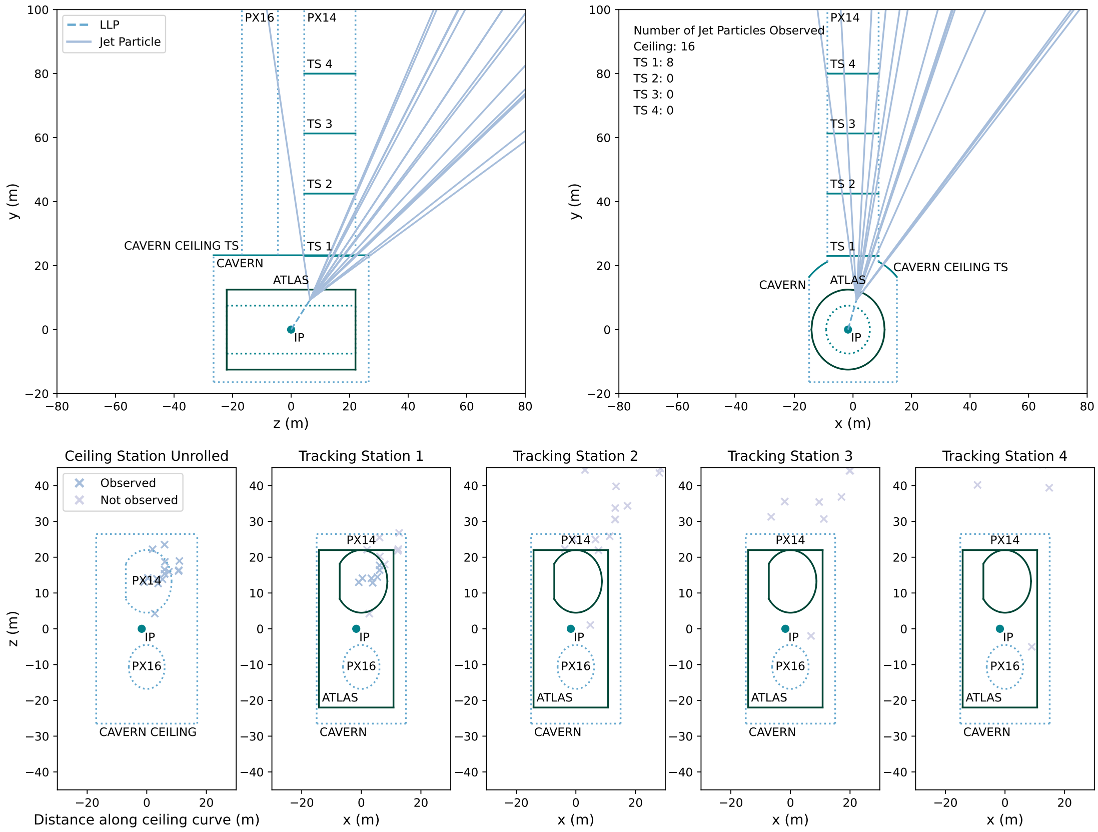


**Figure 5.2:** Event display showing how an in-cavern $K_L^0$-induced event would be observed by ANUBIS in the ceiling and in-shaft configurations. Uses the same format as what is described in the caption of figure 4.3. As shown, 16 final state, charged jet particles would be observed by ANUBIS' ceiling tracking station and 8 would be observed by its first in-shaft tracking station.

of that of the PYTHIA 8 particle. If there are multiple GEANT4 particles with momentum within 50 MeV of the PYTHIA 8 particle, then a particle is randomly selected from these candidates. In order to maximize the number of events whose decay products can be used to study ANUBIS' acceptance, however, a GEANT4 event is randomly selected from those which produce at least two final state, charged jet particles. This event is then weighted by the probability of this occurring, which is the fraction of GEANT4 events within 50 MeV of the PYTHIA 8 particle that produce the requisite number of jet particles. If there are no GEANT4 particles with momentum within 50 MeV, then this threshold is successively increased by 50 MeV until a suitable particle is found. The final state, charged particles generated by the GEANT4 simulation are then considered by the geometric model of ANUBIS using the trajectory given by the PYTHIA 8 event. That is, PYTHIA 8 gives the

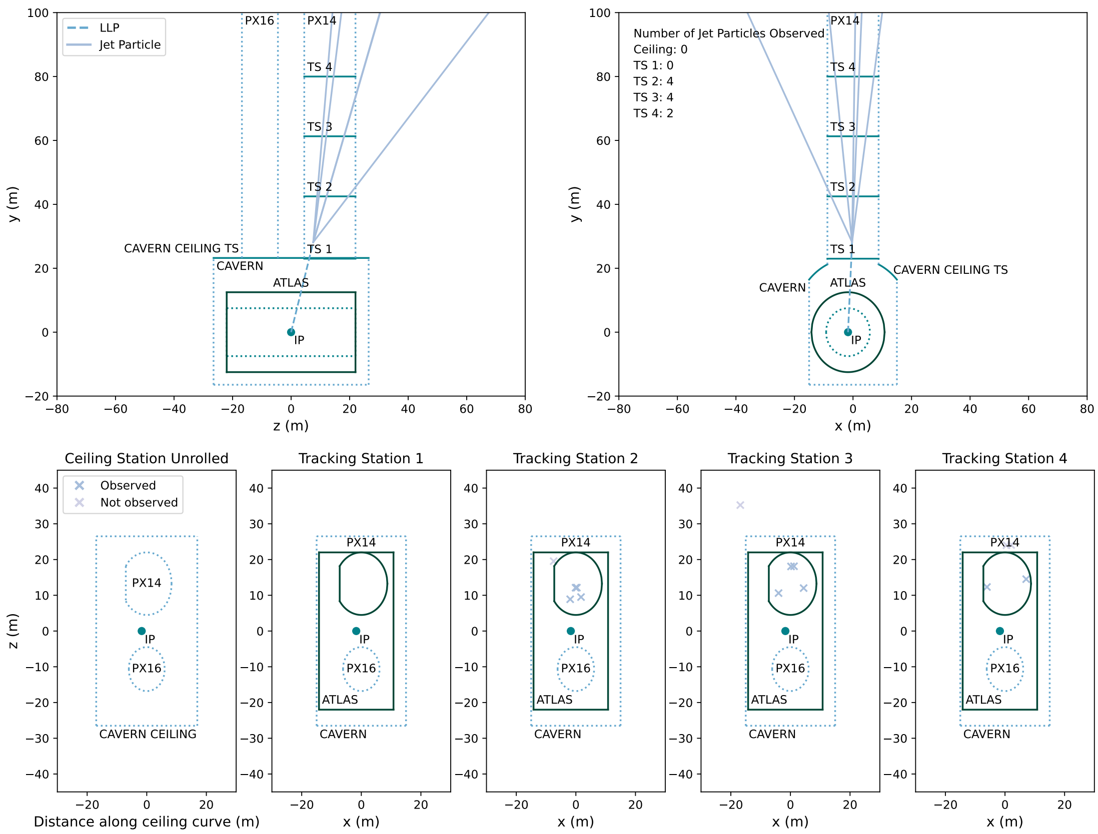


**Figure 5.3:** Event display showing how an in-shaft $n^0$-induced event would be observed by ANUBIS in the shaft configuration. Uses the same format as what is described in the caption of figure 4.3. As shown, 4 final state, charged jet particles would be observed by each of ANUBIS' second and third tracking stations and 2 would be observed by its fourth.

trajectory of the LLP and its event-level information such as $E_T^{\text{miss}}$ and isolation from nearby jets or charged particles, while GEANT4 gives the distance that the particle travels before interacting as well as the spectrum of particles which are produced by that interaction. This simulation only considers interactions with air, ignoring those with detector or cavern material, though it does consider the attenuation of the ATLAS Experiment's calorimeter by applying a corresponding weight to each event. This therefore provides a useful data set for estimating of the number of events with which ANUBIS may have to contend.

## 5.3 Event Selection

These events are scaled in $\varphi$ so that they point towards ANUBIS' tracking stations in an effort to maximize statistics, just as signal Monte Carlo events are, and this is compensated by a weight on each event of $1/2$, which again exploits the symmetry about the ATLAS Experiment's $\varphi$ coordinate. The events are then subject to the same event-level cuts as signal events. Each event must have a $E_T^{\text{miss}} > 30$ GeV, and a $\Delta R$ between the $n^0$ or $K_L^0$ and its nearest reconstructed jet or charged particle in excess of 0.5. As shown in figure 5.4, these cuts significantly attenuate background levels. Critically, these event-level cuts discriminate against a higher fraction of background events than signal events, represented by 10 GeV BSM LLPs with $c\tau = 3$ m, as shown in figure 5.5. The cut on the $\Delta R$ value of the Standard Model LLP and its nearest charged particle has only a slightly more significant effect than the corresponding cut on BSM LLP signal events, however this cut may still be necessary should a potentially imprecise detector necessitate sufficient distance between a reconstructed LLP trajectory and that of a nearby charged particle. Along with the aforementioned probability of traversing the ATLAS Experiment's calorimeter without absorption, the fraction of background LLPs which could interact with ANUBIS is significantly reduced, as shown by the first four cuts in figures 5.4 and 5.5. It is not, however, reduced to zero.

## 5.4 Geometric Model

As before, interactions are considered in two scenarios: in-cavern, relevant to the ceiling and PX14 shaft configurations of ANUBIS, and in-shaft, relevant only to the PX14 shaft configuration. LLPs are assumed to have been produced at the interaction point, and their final state jet particles are assumed to have been produced immediately upon decay. Examples of events in these scenarios can be seen in figures 5.2 and 5.3, respectively. Figure 5.4 demonstrates the effect of requiring ANUBIS acceptance on the number of cut-surviving background events, and this is contrasted with signal events in figure 5.5. As with signal studies, in all ANUBIS configurations and scenarios, an event is considered observed if at least two final state, charged particles with momentum in excess of 100 MeV intersect at least one ANUBIS tracking station. Unlike the signal studies, however, in-shaft interactions of $K_L^0$ or $n^0$ require that the LLP did not pass through the mate-

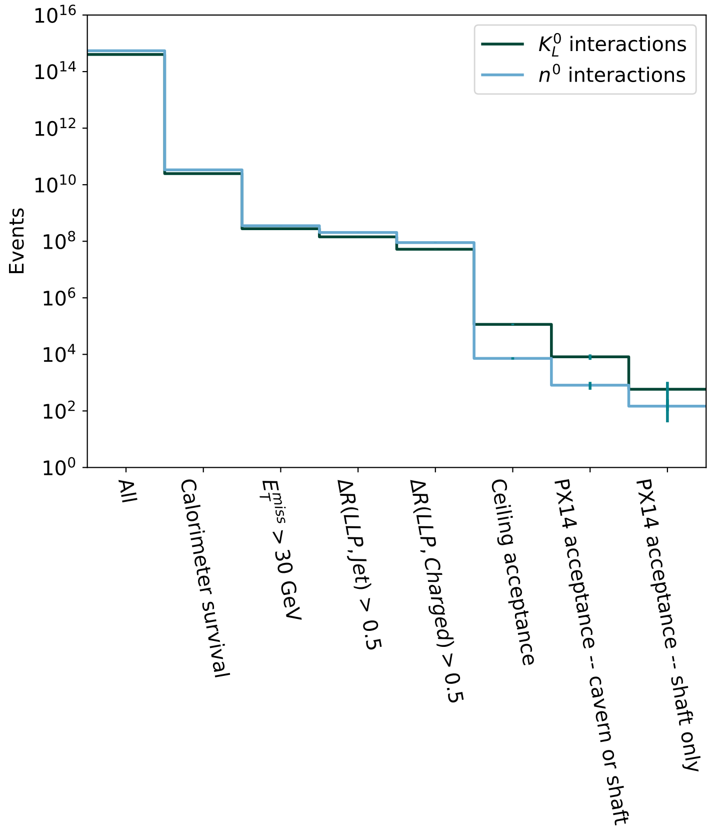


**Figure 5.4:** Cutflow showing the effects of cuts on calorimeter survival, the presence of $E_T^{\text{miss}}$, on LLP isolation, and on ANUBIS acceptance on $K_L^0$ and $n^0$ interactions, scaled to HL-LHC conditions. Note that the final three bins are not cumulative; any event which passes the last event-level cut is separately considered for each detector configuration and decay scenario.

rial surrounding the ATLAS Experiment's cavern, as it is assumed that these particles would have interacted with this material before reaching the PX14 shaft. It should be noted that the final three bins of figures 5.4 and 5.5 are not cumulative; all events which pass the final event-level cut ($\Delta R(\text{LLP}, \text{Charged}) > 0.5$) are separately considered for each of ANUBIS' configurations and scenarios. The cutflow in figure 5.4 has been scaled using the inelastic *pp* cross section of 78.1 mb, calculated for $\sqrt{s} = 13$ TeV, and HL-LHC conditions, $\mathcal{L}_{\text{HL-LHC}} = 3\,\text{ab}^{-1}$.[114]

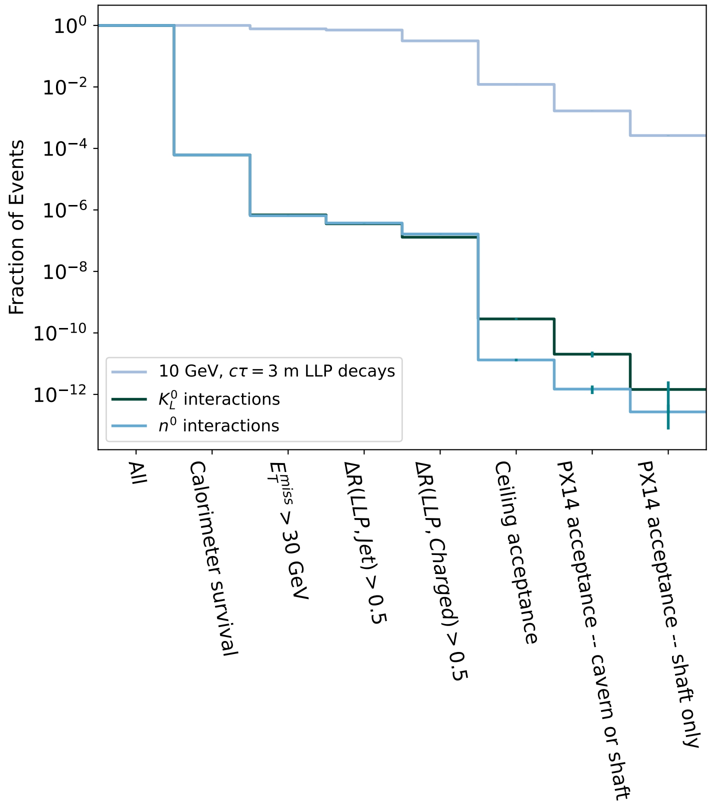


**Figure 5.5:** Cutflow showing the effects of cuts on signal, shown as decays of 10 GeV BSM LLPs with $c\tau = 3$ m, and background, shown as interactions involving $K_L^0$ and $n^0$. Note that the final three bins are not cumulative; any event which passes the last event-level cut is separately considered for each detector configuration and decay scenario.

## 5.5 Results

Clearly, a significant number of $K_L^0$- and $n^0$-induced background events remain, even with the event-level cuts and the requirement for ANUBIS acceptance. $\mathcal{O}(10^5)$ $K_L^0$ and $\mathcal{O}(10^4)$ $n^0$ events can be expected to be observed by ANUBIS' ceiling configuration over the course of the HL-LHC's operation. These numbers are reduced by about one order of magnitude each for ANUBIS' shaft configuration when searching for in-cavern or in-shaft decays to $\mathcal{O}(10^4)$ $K_L^0$ and $\mathcal{O}(10^3)$ $n^0$ events. The number of $K_L^0$- and $n^0$-induced background events is then further reduced by another order of magnitude to $\mathcal{O}(10^3)$ and $\mathcal{O}(10^2)$ such events, respectively, when searching for in-shaft decays only. The uncertainties shown in figures 5.4 and 5.5 are calculated by taking the square root of the sum of the squared weights of the events which are simulated to interact with ANUBIS in a given configuration and scenario in order to estimate $1\sigma$ of the Monte Carlo statistics.

These results show that further investigation is necessary in order to identify novel methods for discriminating against these and other background events. Though the cuts presented in this section do remove a higher proportion of background than signal, as shown in figure 5.5, these background rates indicate that more signal event observations would likely be necessary than those which were used for the studies presented in section 4 in order to eventually claim a significant deviation from the expectation. Recent results from the ATLAS Experiment, such as a search for displaced jets in the experiment's muon spectrometer, have however been able to significantly reduce background events from the rates presented here. [3] For example, that search also considered a LLP's isolation from tracks in the ATLAS Experiment's inner detector or calorimeters, which could have precipitated the background particles. [3] Future studies could investigate the impact of this type of cut on ANUBIS' background acceptance. It is also necessary to validate these results, which largely neglect interactions with the ATLAS Experiment's detector and cavern material. This is the goal of the proANUBIS detector which will soon be installed to the ATLAS Experiment's cavern.

# 6 Conclusion

The ANUBIS project shows exciting potential for detecting new physics. Its detectors, which could be installed either to the ceiling of the ATLAS Experiment's cavern or along its PX14 service shaft, would drastically extend the experiment's sensitivity to the decays of neural BSM LLPs. The project would potentially be sensitive to two decay scenarios: those which occur between the vertexing limit of the ATLAS Experiment's existing detectors and the limits of its cavern, and those which occur within the PX14 service shaft. The work of this thesis shows that when searching for those decays, ANUBIS would have sensitivity to exotic phenomena which far surpasses that of the ATLAS Experiment's existing detectors, and which matches or exceeds that of similar proposals to augment the LHC's experiments.

Using a ceiling configuration of detectors during the HL-LHC, ANUBIS could be sensitive to the decays of 10, 20, 30, and 40 GeV Higgs-portal LLPs with $c\tau$ of 3, 4, 6, and 10 m that are produced with branching ratios reaching $\mathcal{O}(10^{-6})$, assuming no background. This improves upon a result from the ATLAS Experiment and a projection for the MATHUSLA project by more than two orders of magnitude when searching for a 40 GeV Higgs portal LLP. For longer proper lifetimes, ANUBIS continues to outpace the ATLAS Experiment by showing sensitivity to LLPs with $c\tau$ of about $10^5$ m before reaching the excluded branching ratio of Higgs to invisible particle decays, assuming moderate levels of background. The PX14 shaft configuration of ANUBIS also shows promising results, with sensitivity to events with branching ratios about three quarters of an order of magnitude higher when searching for in-cavern or in-shaft decays. This projected sensitivity is raised by another three quarters of an order of magnitude when searching for in-shaft decays only. In the presence of moderate background rates, the ANUBIS project still shows impressive results, reaching sensitivity to branching ratios of $\mathcal{O}(10^{-5})$ in the ceiling configuration and $\mathcal{O}(10^{-4})$ in the shaft configuration for LLPs with $c\tau \approx 5$ m.

The ANUBIS project also shows impressive resilience to background events. Interactions precipitated by $n^0$ and $K_L^0$, which may either decay or interact hadronically with air molecules, are expected to be the most significant sources of background. Event-level cuts alongside attenuation from the ATLAS Experiment's calorimeters reduce the rate of these events by about six orders of magnitude. Requiring acceptance by ANUBIS' detectors further reduces this rate. At HL-LHC conditions, however, this does still leave a significant number of events; $\mathcal{O}(10^5)$ $K_L^0$ and $\mathcal{O}(10^4)$ $n^0$ interactions could be expected to create signals which mimic those of BSM LLPs on ANUBIS' ceiling configuration of detectors. These numbers are each reduced by an order of magnitude for the PX14 shaft configuration of ANUBIS, and they are each reduced by a further order of magnitude when only searching for in-shaft decays. Further work is therefore necessary in order to identify new methods for discriminating against these sources of background.

The ANUBIS project would therefore provide a significant upgrade to the LHC's search for BSM phenomena. At a modest civil engineering cost, when compared to some rival proposals, it could radically extend the ATLAS Experiment's sensitivity to a key class of proposed extensions to the Standard Model of particle physics. As the LHC enters its high-luminosity era, this would help realize the full potential of one of the largest and boldest scientific experiments that has ever been constructed as it seeks to better understand the fundamental laws of our universe.

# A
# Active Volumes of ANUBIS' Configurations

In order to scale the signal requirements for ANUBIS described in section 4, the active volumes of its two configurations must be compared. Given the projection of 50 signal events being necessary to claim detection using ANUBIS' shaft configuration, the ratio of the active volumes of the project's two configurations can provide a good estimate for scaling this projection to the ceiling configuration. The active volume is the region in which a LLP could travel, decay, and be detected by one or more of ANUBIS' tracking stations. It is therefore formed by the cone bounded by the ATLAS Experiment's interaction point and the detectors of ANUBIS' tracking stations. A decay could occur slightly outside of this region and still produce at least two final state, charged jet particles whose trajectories allow them to be detected by ANUBIS' tracking stations, however this event is rare and therefore represents a small number of decays. Restricting to the aforementioned region still provides a reasonable estimate of the relative decay volumes of these configurations.

We begin with the ceiling configuration. The ceiling of the ATLAS Experiment's cavern follows a radius of curvature $r_{\text{curve}} = 20$ m centered at $y_{\text{curve}} = 3.2$ m where $y$ is the vertical coordinate of the cavern and $x$ is the horizontal coordinate ($z$ points along the LHC's beamline).[61] The ceiling's height at a given $x$ position can therefore be given by:

$$y_{\text{curve}} + \sqrt{r_{\text{curve}}^2 - x^2}$$

Knowing that the interaction point, which is the apex of the cone, is located at $\text{IP}_i = (-1.7\text{ m}, 0\text{ m}, 0\text{ m})_i$ in local coordinates, we can integrate over the extent of the cavern's ceiling to find the volume of the cone by considering the Euclidean distance between these points:

$$\int_{z_{\min}}^{z_{\max}} \int_{x_{\min}}^{x_{\max}} \sqrt{(x - \text{IP}_x)^2 + \left(y_{\text{curve}} + \sqrt{r_{\text{curve}}^2 - x^2} - \text{IP}_y\right)^2 + (z - \text{IP}_z)^2}\text{dxdz} =$$
$$\int_{-26.5\text{ m}}^{26.5\text{ m}} \int_{-15\text{ m}}^{15\text{ m}} \sqrt{(x - (-1.7\text{ m}))^2 + \left((3.2\text{ m}) + \sqrt{(20\text{ m})^2 - x^2}\right)^2 + (z)^2}\text{dxdz} = 4.3 \times 10^4\text{ m}^3$$

For the PX14 shaft configuration of ANUBIS, we are considering in-cavern and in-shaft decays, so we begin with a similar approach to find the volume between the interaction point and ANUBIS' first tracking station. ANUBIS' first tracking station begins at $z = 4.5$ m and forms a circle of radius $r_{\text{TS}} = 8.75$ m located at height $y_{\text{TS}} = 23$ m. Here we ignore the cutoff for the pipes which supply the ATLAS Experiment for simplicity. The volume of this cone is therefore given by:

$$\int_{x_{\min}}^{x_{\max}} \int_{z_{\min}+r_{\text{TS}}-\sqrt{r_{\text{TS}}^2-x^2}}^{z_{\min}+r_{\text{TS}}+\sqrt{r_{\text{TS}}^2-x^2}} \sqrt{(x - \text{IP}_x)^2 + \left(y_{\text{TS}} - \text{IP}_y\right)^2 + (z - \text{IP}_z)^2}\text{dzdx} =$$
$$\int_{-8.75\text{ m}}^{8.75\text{ m}} \int_{4.5\text{ m}+8.75\text{ m}-\sqrt{(8.75\text{ m})^2-x^2}}^{4.5\text{ m}+8.75\text{ m}+\sqrt{(8.75\text{ m})^2-x^2}} \sqrt{(x - (-1.7\text{ m}))^2 + (23\text{ m})^2 + (z)^2}\text{dzdx} = 6.5 \times 10^3\text{ m}^3$$

For the subsequent tracking stations, we must consider how the same cone which is bounded by ANUBIS' first tracking station continues into the PX14 service shaft towards the project's other tracking stations. This is necessary because background LLPs' decay products must intersect at least one tracking station, and they are vetoed if they pass through cavern material or earth, so their trajectory must also intersect each of the previous tracking stations. We therefore consider the integral over the coordinate $y$ bounded by tracking station $\mathrm{TS}_i$ and its neighbor below it, $\mathrm{TS}_{i-1}$ for $i \in \{2, 3, 4\}$. At each $y$, we consider the projection of the start of the first tracking station in $z$:

$$y \cdot \frac{z_{\min} - \mathrm{IP}_z}{y_{\mathrm{TS}_1} - \mathrm{IP}_y}$$

As well as the extent of tracking station $\mathrm{TS}_i$ in $z$:

$$y \cdot \frac{z_{\min} + 2 \cdot r_{\mathrm{TS}} - \mathrm{IP}_z}{y_{\mathrm{TS}_i} - \mathrm{IP}_y}$$

We also consider the projection of the extent of the tracking station in $x$ at point $y, z$. This is given by:

$$y \cdot \frac{\sqrt{r_{\mathrm{TS}}^2 - \left(\frac{z-\mathrm{IP}_z}{y-\mathrm{IP}_y} \cdot y_{\mathrm{TS}_i} - r_{\mathrm{TS}} - z_{\min}\right)^2} - \mathrm{IP}_x}{y_{\mathrm{TS}_i} - \mathrm{IP}_y}$$

Where we use the projection in $z$ to compute $x$ at $y_{\mathrm{TS}_i}$, then project this back to $y$. This gives a final double integral for the volume:

$$\int_{y_{\mathrm{TS}_{i-1}}}^{y_{\mathrm{TS}_i}} \int_{y \cdot \frac{z_{\min} - \mathrm{IP}_z}{y_{\mathrm{TS}_1} - \mathrm{IP}_y}}^{y \cdot \frac{z_{\min} + 2 \cdot r_{\mathrm{TS}} - \mathrm{IP}_z}{y_{\mathrm{TS}_i} - \mathrm{IP}_y}} 2 \cdot \frac{\sqrt{r_{\mathrm{TS}}^2 - \left(\frac{z-\mathrm{IP}_z}{y-\mathrm{IP}_y} \cdot y_{\mathrm{TS}_i} - r_{\mathrm{TS}} - z_{\min}\right)^2} - \mathrm{IP}_x}{y_{\mathrm{TS}_i} - \mathrm{IP}_y} \cdot y \, \mathrm{d}z\mathrm{d}y$$

For the volume between ANUBIS' first and second tracking stations, this is:

$$\int_{23\,\mathrm{m}}^{42.5\,\mathrm{m}} \int_{y \cdot \frac{4.5\,\mathrm{m}}{23\,\mathrm{m}}}^{y \cdot \frac{4.5\,\mathrm{m} + 2 \cdot 8.75\,\mathrm{m}}{42.5\,\mathrm{m}}} 2 \cdot \frac{\sqrt{(8.75\,\mathrm{m})^2 - \left(\frac{z}{y} \cdot 42.5\,\mathrm{m} - 8.75\,\mathrm{m} - 4.5\,\mathrm{m}\right)^2} - (-1.7\,\mathrm{m})}{42.5\,\mathrm{m}} \cdot y \, \mathrm{d}z\mathrm{d}y$$
$$= 3.0 \times 10^3\,\mathrm{m}^3$$

For the volume between ANUBIS' second ($y_{\mathrm{TS}_{i-1}} = 42.5\,\mathrm{m}$) and third ($y_{\mathrm{TS}_i} = 61.3\,\mathrm{m}$) tracking stations, this evaluates to $2.4 \times 10^3$ m. For the volume between ANUBIS' third ($y_{\mathrm{TS}_{i-1}} = 61.3\,\mathrm{m}$) and final ($y_{\mathrm{TS}_i} = 80\,\mathrm{m}$) tracking stations, this evaluates to $1.5 \times 10^3$ m. All together, the ratio of active volumes of the two configurations is:

$$\frac{4.3 \times 10^4 \text{ m}^3}{6.5 \times 10^3 \text{ m}^3 + 3.0 \times 10^3 \text{ m}^3 + 2.4 \times 10^3 \text{ m}^3 + 1.5 \times 10^3 \text{ m}^3} = 3.2$$

If we assume that uncertainty on the number of background events is largely statistical, then we can scale the requirement of 50 observations of signal events for the shaft configuration to the ceiling configuration by taking the square root of the ratio of these active volumes. This evaluates to:

$$N_{\text{events}} \cdot \sqrt{\frac{V_{\text{ceiling}}}{V_{\text{shaft}}}} = 50 \cdot \sqrt{3.2} \approx 90$$

# Glossary

$E_T^{\text{miss}}$ Missing energy in the transverse direction.

**ALICE** A large ion collider experiment.

**ANUBIS** An underground belayed in-shaft search experiment.

**ATLAS** A large toroidal LHC apparatus.

**BSM** Beyond the Standard Model.

**CERN** European Organization for Nuclear Research.

**CMS** Compact muon solenoid.

**DAQ** Data acquisition.

**ggF** Gluon fusion.

**HL-LHC** High-Luminosity Large Hadron Collider.

**LHC** Large Hadron Collider.

**LHCb** Large Hadron Collider beauty.

**Linac4** Linear accelerator 4.

**LLP** Long-lived particle.

**MSSM** Minimal Supersymmetric Standard Model.

**proANUBIS** Prototype ANUBIS.

**PS** Proton Synchrotron.

**PSB** Proton Synchrotron Booster.

**RPC** Resistive plate chamber.

**SPS** Super Proton Synchrotron.

**SUSY** Supersymmetry.

**TS** Tracking station.

**VBF** Vector boson fusion.

# References


[1] Aaboud, M. et al. (2016). Measurement of the inelastic proton-proton cross section at $\sqrt{s} = 13$ TeV with the ATLAS detector at the LHC. *Phys. Rev. Lett.*, 117, 182002.

[2] Aaboud, M. et al. (2018). Search for long-lived charginos based on a disappearing-track signature in $pp$ collisions at $\sqrt{s} = 13$ TeV with the ATLAS detector. *Journal of High Energy Physics*, 2018(6).

[3] Aaboud, M. et al. (2019). Search for long-lived particles produced in $pp$ collisions at $\sqrt{s} = 13$ TeV that decay into displaced hadronic jets in the ATLAS muon spectrometer. *Phys. Rev. D*, 99, 052005.

[4] Aad, G. et al. (2012). Observation of a new particle in the search for the Standard Model Higgs boson with the ATLAS detector at the LHC. *Physics Letters B*, 716(1), 1–29.

[5] Aad, G. et al. (2022). Search for neutral long-lived particles in pp collisions at $\sqrt{s} = 13$ TeV that decay into displaced hadronic jets in the ATLAS calorimeter. *Journal of High Energy Physics*, 2022(6).

[6] Aaij, R. et al. (2015). Observation of $J/\psi p$ resonances consistent with pentaquark states in $\Lambda_b^0 \to J/\psi K^- p$ decays. *Physical Review Letters*, 115(7).

[7] Abada, A. et al. (2019). FCC physics opportunities. *The European Physical Journal C*, 79(6), 474.

[8] Agostinelli, S. et al. (2003). GEANT4—a simulation toolkit. *Nuclear Instruments and Methods in Physics Research Section A: Accelerators, Spectrometers, Detectors and Associated Equipment*, 506(3), 250–303.

[9] Aleksa, M. et al. (2013). *ATLAS Liquid Argon Calorimeter Phase-I Upgrade: Technical Design Report*. Technical report. Final version presented to December 2013 LHCC.

[10] Alioli, S., Nason, P., Oleari, C., & Re, E. (2010). A general framework for implementing NLO calculations in shower Monte Carlo programs: the POWHEG BOX. *JHEP*, 06, 043.

[11] Allison, J. et al. (2006). GEANT4 developments and applications. *IEEE Transactions on Nuclear Science*, 53(1), 270–278.

[12] Allison, J. et al. (2016). Recent developments in GEANT4. *Nuclear Instruments and Methods in Physics Research Section A: Accelerators, Spectrometers, Detectors and Associated Equipment*, 835, 186–225.

[13] Alpigiani, C. et al. (2022). Recent progress and next steps for the MATHUSLA LLP detector.

[14] Apollinari, G., Béjar Alonso, I., Brüning, O., Lamont, M., & Rossi, L. (2015). *High-Luminosity Large Hadron Collider (HL-LHC): Preliminary Design Report*. CERN Yellow Reports: Monographs. Geneva: CERN.

[15] Ashie, Y. et al. (2005). Measurement of atmospheric neutrino oscillation parameters by Super-Kamiokande I. *Phys. Rev. D*, 71, 112005.

[16] ATLAS Collaboration (1994). *ATLAS: technical proposal for a general-purpose pp experiment at the Large Hadron Collider at CERN*. LHC technical proposal. Geneva: CERN.

[17] ATLAS Collaboration (1996a). *ATLAS liquid-argon calorimeter: Technical Design Report*. Technical design report. ATLAS. Geneva: CERN.

[18] ATLAS Collaboration (1996b). *ATLAS tile calorimeter: Technical Design Report*. Technical design report. ATLAS. Geneva: CERN.

[19] ATLAS Collaboration (1997a). *ATLAS inner detector: Technical Design Report, 1*. Technical design report. ATLAS. Geneva: CERN.

[20] ATLAS Collaboration (1997b). *ATLAS magnet system: Technical Design Report, 1*. Technical design report. ATLAS. Geneva: CERN.

[21] ATLAS Collaboration (1997c). *ATLAS muon spectrometer: Technical Design Report*. Technical design report. ATLAS. Geneva: CERN.

[22] ATLAS Collaboration (2008). The ATLAS Experiment at the CERN Large Hadron Collider. *Journal of Instrumentation*, 3(08), S08003–S08003.

[23] ATLAS Collaboration (2011). *dE/dx measurement in the ATLAS Pixel Detector and its use for particle identification*. Technical report, CERN, Geneva.

[24] ATLAS Collaboration (2013). Triggers for displaced decays of long-lived neutral particles in the ATLAS detector. *Journal of Instrumentation*, 8(07), P07015–P07015.

[25] ATLAS Collaboration (2014a). *Basic ATLAS TRT performance studies of Run 1*. Technical report, CERN, Geneva.

[26] ATLAS Collaboration (2014b). Operation and performance of the ATLAS semiconductor tracker. *Journal of Instrumentation*, 9(08), P08009–P08009.

[27] ATLAS Collaboration (2015a). Search for long-lived, weakly interacting particles that decay to displaced hadronic jets in proton-proton collisions at $\sqrt{s} = 8$ TeV with the ATLAS detector. *Physical Review D*, 92(1).

[28] ATLAS Collaboration (2015b). Search for pair-produced long-lived neutral particles decaying to jets in the ATLAS hadronic calorimeter in $pp$ collisions at $\sqrt{s} = 8$ TeV. *Physics Letters B*, 743, 15–34.

[29] ATLAS Collaboration (2017a). *ATLAS Liquid Argon Calorimeter Phase-II Upgrade: Technical Design Report*. Technical report, CERN, Geneva.

[30] ATLAS Collaboration (2017b). Performance of the ATLAS trigger system in 2015. *The European Physical Journal C*, 77(5).

[31] ATLAS Collaboration (2017c). *Technical Design Report for the ATLAS Inner Tracker Pixel Detector*. Technical report, CERN, Geneva.

[32] ATLAS Collaboration (2017d). *Technical Design Report for the Phase-II Upgrade of the ATLAS Muon Spectrometer*. Technical report, CERN, Geneva.

[33] ATLAS Collaboration (2017e). *Technical Design Report for the Phase-II Upgrade of the ATLAS TDAQ System*. Technical report, CERN, Geneva.

[34] ATLAS Collaboration (2017f). *Technical Design Report for the Phase-II Upgrade of the ATLAS Tile Calorimeter*. Technical report, CERN, Geneva.

[35] ATLAS Collaboration (2018). Search for the Higgs boson produced in association with a vector boson and decaying into two spin-zero particles in the $H \rightarrow aa \rightarrow 4b$ channel in *pp* collisions at $\sqrt{s} = 13$ TeV with the ATLAS detector. *Journal of High Energy Physics*, 2018(10).

[36] ATLAS Collaboration (2019a). Search for long-lived particles in final states with displaced dimuon vertices in *pp* collisions at $\sqrt{s} = 13$ TeV with the ATLAS detector. *Physical Review D*, 99(1).

[37] ATLAS Collaboration (2019b). *Standard Model Summary Plots Spring 2019*. Technical report, CERN, Geneva.

[38] ATLAS Collaboration (2020). Operation of the ATLAS trigger system in Run 2. *Journal of Instrumentation*, 15(10), P10004–P10004.

[39] ATLAS Collaboration (2021). *Constraining the Dark Sector with the monojet signature in the ATLAS experiment*. Technical report, CERN, Geneva.

[40] ATLAS Collaboration (2022). Search for events with a pair of displaced vertices from long-lived neutral particles decaying into hadronic jets in the ATLAS muon spectrometer in pp collisions at $\sqrt{s} = 13$ TeV.

[41] ATLAS Collaboration (2022). Search for heavy, long-lived, charged particles with large ionisation energy loss in *pp* collisions at $\sqrt{s} = 13$ TeV using the ATLAS Experiment and the full Run 2 dataset.

[42] Bandurin, D. et al. (2015). Review of physics results from the Tevatron. *International Journal of Modern Physics A*, 30(06), 1541001.

[43] Bauer, M., Brandt, O., Lee, L., & Ohm, C. (2019). ANUBIS: Proposal to search for long-lived neutral particles in CERN service shafts.

[44] Bayatian, G. L. et al. (2006). *CMS Physics: Technical Design Report Volume 1: Detector Performance and Software*. Technical design report. CMS. Geneva: CERN.

[45] Bernaciak, C., Plehn, T., Schichtel, P., & Tattersall, J. (2015). Spying an invisible Higgs boson. *Physical Review D*, 91(3).

[46] Bertone, G. & Hooper, D. (2018). History of dark matter. *Rev. Mod. Phys.*, 90, 045002.

[47] Brice, M. (2008). Aerial View of the CERN taken in 2008.

[48] Brüning, O. S. et al. (2004). *LHC Design Report*. CERN Yellow Reports: Monographs. Geneva: CERN.

[49] Buttinger, W. (2012). The ATLAS level-1 trigger system. *Journal of Physics: Conference Series*, 396(1), 012010.

[50] Cacciari, M., Salam, G. P., & Soyez, G. (2012). FastJet user manual. *The European Physical Journal C*, 72(3).

[51] Carlip, S. (2001). Quantum gravity: a progress report. *Reports on Progress in Physics*, 64(8), 885–942.

[52] Chan, Y. F., Low, M., Morrissey, D. E., & Spray, A. P. (2012). LHC signatures of a minimal supersymmetric hidden valley. *Journal of High Energy Physics*, 2012(5).

[53] Chang, S., Dermíšek, R., Gunion, J. F., & Weiner, N. (2008). Nonstandard Higgs boson decays. *Annual Review of Nuclear and Particle Science*, 58(1), 75–98.

[54] Chang, S., Fox, P. J., & Weiner, N. (2006). Naturalness and higgs decays in the MSSM with a singlet. *Journal of High Energy Physics*, 2006(08), 068–068.

[55] Chou, J. P., Curtin, D., & Lubatti, H. (2017). New detectors to explore the lifetime frontier. *Physics Letters B*, 767, 29–36.

[56] CMS Collaboration (2015). Search for long-lived particles that decay into final states containing two electrons or two muons in proton-proton collisions at $\sqrt{s} = 8$ TeV. *Physical Review D*, 91(5).

[57] Correia, H. & Maria, A. (2015). *The ATLAS Tile Calorimeter*. Technical report, CERN, Geneva.

[58] Curtin, D. et al. (2014). Exotic decays of the 125 GeV Higgs boson. *Physical Review D*, 90(7).

[59] Curtin, D. et al. (2019). Long-lived particles at the energy frontier: the MATHUSLA physics case. *Reports on Progress in Physics*, 82(11), 116201.

[60] Damerau, H. et al. (2014). *LHC Injectors Upgrade, Technical Design Report*.

[61] Dawson, I. & Hedberg, V. (2004). *Radiation in the USA15 cavern in ATLAS*. Technical report, CERN, Geneva.

[62] Diehl, E. (2009). ATLAS muon detector commissioning.

[63] Dine, M. & Kusenko, A. (2003). Origin of the matter-antimatter asymmetry. *Rev. Mod. Phys.*, 76, 1–30.

[64] Fradette, A. & Pospelov, M. (2017). BBN for the LHC: Constraints on lifetimes of the Higgs portal scalars. *Phys. Rev. D*, 96, 075033.

[65] Frixione, S., Nason, P., & Oleari, C. (2007). Matching NLO QCD computations with Parton Shower simulations: the POWHEG method. *JHEP*, 11, 070.

[66] Fujii, K. et al. (2015). Physics case for the International Linear Collider.

[67] Gligorov, V. V., Knapen, S., Papucci, M., & Robinson, D. J. (2018). Searching for long-lived particles: A compact detector for exotics at LHCb. *Phys. Rev. D*, 97, 015023.

[68] Green, D. (2010). *At The Leading Edge: The ATLAS and CMS LHC Experiments*. World Scientific Publishing Company.

[69] Griffiths, D. (1987). *Introduction to Elementary Particles*. Wiley.

[70] Hall, L. J., Jedamzik, K., March-Russell, J., & West, S. M. (2010). Freeze-in production of FIMP dark matter. *Journal of High Energy Physics*, 2010(3).

[71] Haywood, S., Rossi, L., Nickerson, R., & Romaniouk, A. (1997). *ATLAS inner detector: Technical Design Report, 2*. Technical design report. ATLAS. Geneva: CERN.

[72] Herr, W. & Muratori, B. (2006). Concept of luminosity.

[73] Kawamoto, T. et al. (2013). *New Small Wheel Technical Design Report*. Technical report.

[74] Koppenburg, P. (2021). List of hadrons observed at the LHC.

[75] Landua, F. (2022). The CERN accelerator complex layout in 2022. Complexe des accélérateurs du CERN en janvier 2022. General Photo.

[76] Lee, L., Ohm, C., Soffer, A., & Yu, T.-T. (2019). Collider searches for long-lived particles beyond the Standard Model. *Progress in Particle and Nuclear Physics*, 106, 210–255.

[77] Lees, J. P. et al. (2015). Search for long-lived particles in $e^+e^-$ collisions. *Physical Review Letters*, 114(17).

[78] LHCb Collaboration (2013). First observation of CP violation in the decays of $B_s^0$ mesons. *Physical Review Letters*, 110(22).

[79] LHCb Collaboration (2014). Observation of the resonant character of the $Z(4430)^-$ state. *Physical Review Letters*, 112(22).

[80] LHCb Collaboration (2021). Test of lepton universality in beauty-quark decays.

[81] Martin, S. P. (1998). A supersymmetry primer. In *Perspectives on Supersymmetry* (pp. 1–98). World Scientific.

[82] Mindur, B. (2016). *ATLAS Transition Radiation Tracker (TRT): Straw tubes for tracking and particle identification at the Large Hadron Collider*. Technical report, CERN, Geneva.

[83] Morgan, J. (2013). Higgs boson scientists win Nobel prize in physics. *BBC News*.

[84] Nagai, K. (1996). Thin gap chambers in ATLAS. *Nuclear Instruments and Methods in Physics Research Section A: Accelerators, Spectrometers, Detectors and Associated Equipment*, 384(1), 219–221.

[85] Nason, P. (2004). A New method for combining NLO QCD with shower Monte Carlo algorithms. *JHEP*, 11, 040.

[86] Pequenao, J. (2008a). Computer Generated image of the ATLAS calorimeter.

[87] Pequenao, J. (2008b). Computer generated image of the ATLAS inner detector.

[88] Pequenao, J. (2008c). Computer generated image of the ATLAS muons subsystem.

[89] Pequenao, J. (2008d). Computer generated image of the whole ATLAS detector.

[90] Pequenão, J. & Maio, A. (2002). Virtual reality image of ATLAS with cavern walls and shafts visible. Image en realite virtuelle de la caverne ATLAS avec ses murs et ses puits visibles. ATLAS Collection.

[91] Pernegger, H. (2015). *The Pixel Detector of the ATLAS Experiment for LHC Run-2*. Technical report, CERN, Geneva.

[92] Petraki, K. & Volkas, R. R. (2013). Review of asymmetric dark matter. *International Journal of Modern Physics A*, 28(19), 1330028.

[93] Rossi, L. (2003). The LHC superconducting magnets. *Proceedings of the 2003 Particle Accelerator Conference*, 1, 141–145 Vol.1.

[94] Rosso, A. D. (2015). Tracking the LHC halo. Suivre le halo du LHC à la trace. (pp.4).

[95] Sjöstrand, T. et al. (2015). An introduction to PYTHIA 8.2. *Computer Physics Communications*, 191, 159–177.

[96] Strassler, M. J. & Zurek, K. M. (2007). Echoes of a hidden valley at hadron colliders. *Physics Letters B*, 651(5), 374–379.

[97] Strassler, M. J. & Zurek, K. M. (2008). Discovering the Higgs through highly-displaced vertices. *Physics Letters B*, 661(4), 263–267.

[98] Tumasyan, A. et al. (2021). Search for long-lived particles decaying in the CMS end cap muon detectors in proton-proton collisions at $\sqrt{s} = 13$ Tev. *Physical Review Letters*, 127(26).

[99] Vazquez, W. P. (2017). The ATLAS data acquisition system in LHC Run 2. *Journal of Physics: Conference Series*, 898, 032017.

[100] Wermes, N. & Hallewel, G. (1998). *ATLAS pixel detector: Technical Design Report*. Technical design report. ATLAS. Geneva: CERN.

[101] Zhang, H. (2011). The ATLAS liquid argon calorimeter: Overview and performance. *Journal of Physics: Conference Series*, 293, 012044.

[102] Zyla, P.A. and others (2020). Review of Particle Physics. *Progress of Theoretical and Experimental Physics*, 2020(8). 083C01.